
PointTruss: K-Truss for Point Cloud Registration

Yue Wu^{1,2} **Jun Jiang**^{1,2} **Yongzhe Yuan**^{1,2} **Maoguo Gong**^{1,3,5*}
Qiguang Miao^{1,2} **Hao Li**^{1,3} **Mingyang Zhang**^{1,3} **Wenping Ma**⁴

¹MoE Key Lab of Collaborative Intelligence Systems, Xidian University

²School of Computer Science and Technology, Xidian University

³School of Electronic Engineering, Xidian University

⁴School of Artificial Intelligence, Xidian University

⁵Academy of AI, College of Mathematics Science, Inner Mongolia Normal University
{ywu, qgmiao, haoli, myzhang, wpma}@xidian.edu.cn, gong@ieee.org,
xiaolongfan@outlook.com, {junj, yyz}@stu.xidian.edu.cn

Abstract

Point cloud registration is a fundamental task in 3D computer vision. Recent advances have shown that graph-based methods are effective for outlier rejection in this context. However, existing clique-based methods impose overly strict constraints and are NP-hard, making it difficult to achieve both robustness and efficiency. While the k -core reduces computational complexity, which only considers node degree and ignores higher-order topological structures such as triangles, limiting its effectiveness in complex scenarios. To overcome these limitations, we introduce the k -truss from graph theory into point cloud registration, leveraging triangle support as a constraint for inlier selection. We further propose a consensus voting-based low-scale sampling strategy to efficiently extract the structural skeleton of the point cloud prior to k -truss decomposition. Additionally, we design a spatial distribution score that balances coverage and uniformity of inliers, preventing selections that concentrate on sparse local clusters. Extensive experiments on KITTI, 3DMatch, and 3DLoMatch demonstrate that our method consistently outperforms both traditional and learning-based approaches in various indoor and outdoor scenarios, achieving state-of-the-art results.

1 Introduction

Point cloud registration is a fundamental problem in 3D computer vision [43, 29], remote sensing [19, 12], 3D reconstruction [6, 11], and autonomous driving [50]. Its primary goal is to estimate the optimal rigid transformation matrix that precisely aligns two point clouds. Accurate 3D correspondences form the foundation of point cloud registration. High-quality correspondences enable the correct computation of rotation and translation, and their quality directly affects the final registration accuracy.

Recent works [48, 1] demonstrate the effectiveness of graph theory for correspondences selection in point cloud registration. In a graph, vertices represent matched point pairs, and edges encode geometric compatibility, which are added when two correspondences meet a pre-set threshold [30]. Based on this representation, several graph algorithms have been developed to select reliable correspondences. The classical maximal clique approach [49, 37] seeks reliable matches by finding fully connected subgraphs, ensuring strong geometric consistency but facing two major challenges. The strict connectivity is often unachievable due to noise or occlusion, resulting in the loss of correct matches. Maximal clique search is NP-hard [13], making it impractical for large-scale data. The k -core method [35, 32] relaxes connec-

*Corresponding author.

tivity requirements and reduces computation, but its weak constraints compromise correspondences reliability, which highlights the difficulty in balancing structural robustness and efficiency. To address these limitations, we introduce the k -truss concept from community detection [47, 46, 26] into point cloud registration. A k -truss [9] requires each edge to participate in at least $k-2$ triangles, leveraging the rigidity and invariance of triangles. Triangles derive their strength from their stable structure, serving as the simplest rigid planar formation and preserving their geometric properties regardless of rotation or translation. In real-world data, inlier correspondences naturally form triangle-rich clusters, as shown in Fig. 1, making k -truss decomposition effective for preserving reliable matches while filtering outliers. Our method first uses consensus voting for low-scale sampling, then constructs a compatibility graph and applies k -truss decomposition. For each resulting subgraph, we estimate the transformation via weighted SVD [7] and rank candidates using a spatial distribution score, selecting the transformation with the highest score as the final result.

To our knowledge, this is the first work to introduce k -truss into point cloud registration, establishing a robust correspondences selection framework based on triangle constraints. Inspired by k -truss, we propose a heuristic method that leverages triangle-based truss structures to robustly filter and refine correspondences. Experimental results show that our method achieves excellent performance under high noise and outlier ratios. Meanwhile, it maintains polynomial time complexity and demonstrates high computational efficiency among graph-based methods. Extensive evaluations on standard datasets further demonstrate that our method significantly outperforms existing state-of-the-art approaches in registration accuracy. Our main contributions are summarized as follows:

- We propose a novel correspondence selection method called PointTruss. It uses triangle support constraints to effectively filter out mismatches related to isolated and low-support edges.
- We develop an integrated pipeline. It applies consensus-voting low-scale sampling to extract the structural skeleton, k -truss decomposition to preserve triangle-supported inliers, and spatial distribution scoring to favor broad, uniform coverage. Each component is modular and can be used independently.
- Extensive experiments on KITTI, 3DMatch, and 3DLoMatch show that PointTruss consistently outperforms both traditional and learning-based methods across diverse indoor and outdoor scenarios. It achieves state-of-the-art accuracy and efficiency with polynomial-time complexity and strong robustness to noise and outliers.

2 Related Work

Traditional Point Cloud Registration. RANSAC and its variants [14, 2] iteratively sample from the initial correspondence set to find the largest consensus set. Early handcrafted feature descriptors, such as FPFH [31], extract local features by encoding geometric histograms. FGR [51] estimates the optimal transformation using robust estimators like the Geman-McClure loss. Branch-and-bound (BnB) based optimization methods, such as GORE [3] and its variant QGORE [25], perform global search in the parameter space to obtain the best transformation. Voting-based method [40] select reliable correspondences through a scoring mechanism. Some works tackle registration with high outlier rates and non-convex objectives via robust and global search, mitigating local minima and improving convergence [28, 34]. However, these methods often suffer from low computational efficiency and limited accuracy under high outlier ratios.

Learning-based Point Cloud Registration. Current learning-based point cloud registration approaches can be categorized as follows. The first category focuses on detecting reliable keypoints or extracting more discriminative features [29, 41]. For example, FCGF [8] uses a fully convolutional network to extract point cloud features in a single pass, without separate keypoint detection. Another category aims to distinguish inliers from outliers. PointDSC [1] removes outliers using pairwise spatial compatibility supervision, while VBReg [20] introduces variational non-local networks for

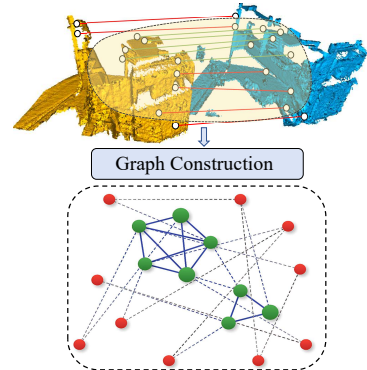


Figure 1: Triangular structure as inlier indicator. Inlier correspondences (green) form triangle-rich structures, while outliers (red) lack triangular support.

outlier rejection. There are also end-to-end approaches [42], such as Deep Global Registration (DGR) [7], which employs sparse convolution and point-wise MLPs to classify correspondences. Although these methods perform well in specific scenarios [44], they generally require large amounts of training data and have limited generalization ability. In contrast, training-free graph-based registration methods often exhibit better robustness and can be integrated as auxiliary modules in deep learning frameworks to further improve overall performance.

Graph-based Point Cloud Registration. Graph-based algorithms [30] typically construct a compatibility graph by evaluating the pairwise compatibility of correspondences, which enables efficient removal of a large number of outliers. For example, the TEASER [39] employs maximal clique theory to decouple scale, rotation, and translation estimation. ROBIN [32] uses the maximal k-core theory for outlier pruning. SUCOFT [35] introduces the concept of k-supercore to improve outlier rejection effectiveness. SC²-PCR [5] imposes stricter constraints on correspondences by introducing a second-order spatial compatibility metric. MAC [48] first proposes a maximal clique-based method to mine richer local consistency information, while FastMAC [49] accelerates computation by applying random spectral sampling on the correspondence graph. These methods demonstrate that mining key information in the compatibility graph is crucial for improving the robustness and accuracy of point cloud registration.

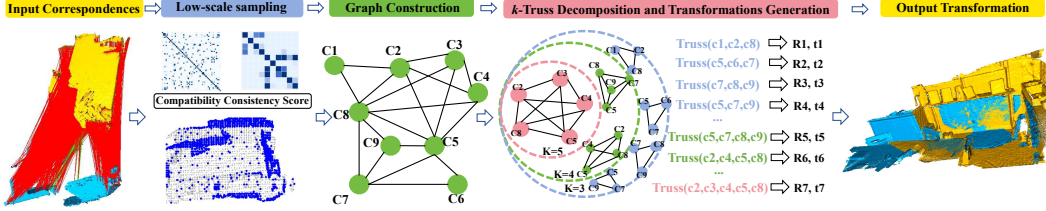


Figure 2: **Pipeline of our method.** 1. Starting from input correspondences, perform low-scale sampling to reduce redundancy. 2. Constructing a correspondence graph and apply k -truss decomposition to identify subgraphs with varying levels of triangle support (i.e., different k values). 3. Each k -truss subgraph represents a set of correspondences with a specific degree of structural consistency. 4. Based on these subgraphs, generate multiple transformation hypotheses and select the optimal transformation using the spatial distribution score.

3 Methods

3.1 Problem Formulation

For two point clouds, where the source point cloud is defined as $\mathbf{P} = \{\mathbf{p}_i \in \mathbb{R}^3 \mid i = 1, \dots, N\}$ and the target point cloud as $\mathbf{Q} = \{\mathbf{q}_i \in \mathbb{R}^3 \mid i = 1, \dots, M\}$, the goal of point cloud registration is to estimate the rigid transformation $\mathbf{T} = \{\mathbf{R}, \mathbf{t}\}$ that aligns these two point clouds. Here, $\mathbf{R} \in SO(3)$ represents the rotation matrix, and $\mathbf{t} \in \mathbb{R}^3$ represents the translation vector. The optimization problem can be formulated as:

$$\min_{\mathbf{R}, \mathbf{t}} \sum_{(\mathbf{p}_i, \mathbf{q}_i) \in \mathcal{C}} \|\mathbf{R}\mathbf{p}_i + \mathbf{t} - \mathbf{q}_i\|_2^2, \quad (1)$$

where $\mathcal{C} = \{\mathbf{c}_i \mid i = 1, \dots, N_c\}$ is the initial correspondence set obtained through feature matching, with each correspondence $\mathbf{c}_i = (\mathbf{p}_i, \mathbf{q}_i)$.

We extract either geometric or learned local features from the point clouds, use feature matching to generate \mathcal{C} , and apply the k -truss method to extract the optimal subgraph. This subgraph is then used to estimate the six degrees of freedom (6-DoF) pose transformation between \mathbf{P} and \mathbf{Q} . The overall pipeline is illustrated in Fig. 2, and the PointTruss is both simple and efficient.

3.2 Graph Construction

The graph space can more accurately capture the affinity relationships between correspondences than Euclidean space [5]. Therefore, we represent the initial correspondences as a compatibility

graph, where each node denotes a correspondence and edges connect nodes that are geometrically compatible [1, 23, 24, 30, 48].

The graph is constructed using the rigid distance constraint between correspondence pairs $(\mathbf{c}_i, \mathbf{c}_j)$, which is quantitatively measured as:

$$S_{dist}(\mathbf{c}_i, \mathbf{c}_j) = \|\|\mathbf{p}_i - \mathbf{p}_j\| - \|\mathbf{q}_i - \mathbf{q}_j\|\| \leq 2\tau, \quad (2)$$

where $\tau = c \cdot \sigma$ is the distance threshold, c is typically set to 3.5 based on statistical confidence intervals, and σ is the standard deviation of noise, which controls the sensitivity to distance discrepancies. This constraint ensures that the distance between point pairs remains nearly invariant under rigid transformations.

The compatibility consistency score between \mathbf{c}_i and \mathbf{c}_j is defined as:

$$S_{comp}(\mathbf{c}_i, \mathbf{c}_j) = \exp\left(-\frac{S_{dist}(\mathbf{c}_i, \mathbf{c}_j)^2}{2\sigma^2}\right), \quad (3)$$

If $S_{comp}(\mathbf{c}_i, \mathbf{c}_j)$ exceeds a threshold τ_{comp} , an edge \mathbf{e}_{ij} is formed between \mathbf{c}_i and \mathbf{c}_j . The weight of the edge is $S_{comp}(\mathbf{c}_i, \mathbf{c}_j)$. Otherwise, $S_{comp}(\mathbf{c}_i, \mathbf{c}_j)$ is set to zero.

3.3 Consensus Voting-based Low-scale Sampling Strategy

To efficiently identify inlier correspondences and reduce the search space, we propose a consensus voting-based low-scale sampling strategy. This method leverages the previously defined geometric consistency metrics to identify the most reliable correspondences.

Consensus Score Computation. Utilizing the compatibility score S_{comp} defined in Eq. (3), we compute the consensus score for each correspondence i by counting the number of other correspondences that are geometrically compatible with it:

$$S_i = \sum_{j=1, j \neq i}^N \mathbb{I}(S_{comp}(\mathbf{c}_i, \mathbf{c}_j) > \tau_c), \quad (4)$$

where $\mathbb{I}(\cdot)$ is the indicator function and τ_c is the consistency threshold. This score represents the number of other correspondences that support correspondence i .

Non-Maximum Suppression. To avoid sampling spatially clustered correspondences, we apply non-maximum suppression [27]:

$$\text{IsLocalMax}_i = \min_{j \in \mathcal{N}} ((S_i \geq S_j) \vee (d_{ij}^s \geq r_{nms})), \quad (5)$$

where \mathcal{N} is the set of all correspondences, $d_{ij}^s = \|\mathbf{p}_i - \mathbf{p}_j\|_2$ is the Euclidean distance between source points, r_{nms} is the non-maximum suppression radius, and \vee denotes the logical OR operation. A correspondence is considered a local maximum when, for all other correspondences, either its score is higher or it is spatially distant.

The final score for each correspondence is:

$$S_i^{\text{final}} = S_i \cdot \text{IsLocalMax}_i, \quad (6)$$

Low-scale Sampling. We select the top- K correspondences with the highest final scores, where K is determined by:

$$K = \lfloor \beta \cdot \mathcal{N} \rfloor, \quad (7)$$

with β being the sampling ratio parameter. This sampling strategy ensures that we can select a diverse set of geometrically consistent correspondences, significantly reducing the computational cost of subsequent operations while maintaining a high probability of including correct correspondences.

3.4 The k -Truss Decomposition

Following the Consensus Voting-based Low-scale Sampling Strategy presented in Sec. 3.3, we construct a new compatibility graph among the selected high-quality correspondences. The adjacency matrix \mathbf{A} of this refined graph represents the pairwise geometric consistency relationships established in Sec. 3.2, but now focused on the reduced set of promising correspondences. To further identify structurally consistent subsets, we apply k -truss decomposition to this adjacency matrix.

Definition 1. (*k -Truss Decomposition Theory*). *Given an undirected graph $G = (V, E)$ and an integer $k \geq 3$, the k -truss of G , denoted by $T_k(G)$, is defined as the maximal subgraph $H = (V_H, E_H)$ of G where every edge $e \in E_H$ is contained in at least $(k - 2)$ triangles within H .*

This formal definition captures the essential property that each edge in a k -truss must have strong structural support through triangle formations. In the context of correspondence graphs, a triangle represents three correspondences that are mutually consistent, which is a stronger constraint than pairwise consistency.

Definition 2. (*Triangle Support*). *For an edge $e = (u, v) \in E$ in a graph $G = (V, E)$, the triangle support of e , denoted by $\text{sup}(e, G)$, is defined as the number of triangles in G that contain e :*

$$\text{sup}(e, G) = |\{w \in V \setminus \{u, v\} : (u, w) \in E \wedge (v, w) \in E\}|, \quad (8)$$

The triangle support can be efficiently computed using matrix operations. If \mathbf{A} is the adjacency matrix of G , then:

$$\text{sup}((u, v), G) = (\mathbf{A}^2)_{u,v} \cdot \mathbf{A}_{u,v}, \quad (9)$$

where $(\mathbf{A}^2)_{u,v}$ counts the number of length-2 paths between u and v .

Theorem 1. *Let (p_i, p_j, p_k) denote a triplet of point correspondences, and let ΔD_{ijk} represent the deviation vector of triangle edge lengths between the source and target point clouds. Under a rigid transformation with Gaussian noise, for any threshold $\epsilon > 0$,*

$$\mathbb{P}(\|\Delta D_{ijk}\|_F < \epsilon \mid \text{correct}) \gg \mathbb{P}(\|\Delta D_{ijk}\|_F < \epsilon \mid \text{incorrect}),$$

where $\mathbb{P}(\cdot)$ denotes the probability, $\|\Delta D_{ijk}\|_F$ denotes the Frobenius norm of the deviation vector, and \gg indicates "significantly greater than." This inequality states that the probability of triangle relationships being preserved under rigid transformation is significantly higher for correct correspondences than for incorrect ones.

Therefore, the k -truss, which requires each edge to be supported by at least $k - 2$ triangles, significantly enhances robustness in correspondence selection by leveraging higher-order structural consistency.

Please see Appendix A.2 for detailed proof and derivations.

Matrix-Based Implementation. The k -truss decomposition operates on the adjacency matrix derived from the sampled correspondences. The algorithm proceeds by computing the triangle support for each edge:

$$\mathbf{T} = \mathbf{A}^2 \odot \mathbf{A}, \quad (10)$$

where \odot denotes the Hadamard (element-wise) product.

We then identify valid edges that satisfy the k -truss criterion [9]:

$$\mathbf{E}_{\text{valid}} = (\mathbf{T} \geq (k - 2)), \quad (11)$$

For each vertex i , we extract its neighborhood connected by valid edges:

$$\mathcal{N}_i = \{j \in V : \mathbf{E}_{\text{valid}}(i, j) = 1\}, \quad (12)$$

Vertices with neighborhoods of sufficient size ($|\mathcal{N}_i| \geq k$) form clusters in the k -truss decomposition.

Computational Complexity Analysis of k -Truss Decomposition. The k -truss decomposition has a time complexity of $O(m^{1.5})$, which is much more efficient than exponential-time clique-based methods and remains practical for large-scale graphs. For more details, please refer to Appendix A.3.

3.5 Hypothesis Generation and Evaluation

Each k -truss subgraph filtered from the previous step represents a structurally robust set of correspondences. By applying the SVD algorithm to each k -truss subgraph, we can obtain a set of 6-DoF pose hypotheses.

Centrality-weighted SVD. Transformation estimation of correspondences is implemented using weighted SVD [48, 29, 5, 7]. We assign weights to correspondences based on their centrality values within the k -truss subgraph. Our weighting scheme follows established graph-based PCR methods by deriving weights from spectral analysis [24]. We compute the eigendecomposition of the k -truss subgraph’s compatibility matrix and use the principal eigenvector elements as correspondence weights in our weighted SVD. This method leverages the structural importance of each correspondence to improve transformation accuracy.

The final goal of our method is to estimate the optimal 6-DoF rigid transformation (composed of a rotation pose $\mathbf{R}^* \in SO(3)$ and a translation pose $\mathbf{t}^* \in \mathbb{R}^3$) that maximizes our spatial distribution score function:

$$(\mathbf{R}^*, \mathbf{t}^*) = \arg \max_{\mathbf{R}, \mathbf{t}} SDS(\mathbf{P}, \mathbf{Q}, \mathbf{R}, \mathbf{t}), \quad (13)$$

where SDS represents our spatial distribution score function defined as:

$$SDS(\mathbf{P}, \mathbf{Q}, \mathbf{R}, \mathbf{t}) = \rho_{\text{inlier}} \cdot \sqrt{\rho_{\text{coverage}}} \cdot \rho_{\text{error}}, \quad (14)$$

with the individual components:

$$\rho_{\text{inlier}} = \frac{|\mathcal{I}|}{|\mathbf{P}|}, \quad (15)$$

$$\rho_{\text{coverage}} = \frac{\prod_{d \in \{x, y, z\}} \text{range}_d(\mathcal{I})}{\prod_{d \in \{x, y, z\}} \text{range}_d(\mathbf{P})}, \quad (16)$$

$$\rho_{\text{error}} = 1 - \frac{\frac{1}{|\mathcal{I}|} \sum_{i \in \mathcal{I}} \|\mathbf{R}\mathbf{p}_i + \mathbf{t} - \mathbf{q}_i\|}{\tau}, \quad (17)$$

where $\mathcal{I} = \{i : \|\mathbf{R}\mathbf{p}_i + \mathbf{t} - \mathbf{q}_i\| < \tau\}$ is the set of inlier indices, τ is the inlier threshold, range_d computes the coordinate range along dimension d , $\mathbf{p}_i \in \mathbf{P}$ and $\mathbf{q}_i \in \mathbf{Q}$ are corresponding points from source and target point clouds.

Unlike conventional metrics such as MAE [48] or inlier count [5], our SDS function comprehensively evaluates both alignment accuracy and spatial distribution quality of inliers. The ρ_{inlier} term measures the proportion of correctly aligned points, ρ_{coverage} evaluates how well the inliers span the original point cloud volume, and ρ_{error} assesses the precision of alignment among inlier points. This balanced evaluation method effectively prevents selecting transformations with clustered inliers in limited regions and promotes transformations with well-distributed inliers across the entire object. The best hypothesis according to this comprehensive scoring function is selected to perform the final 3D registration.

4 Experiment

4.1 Experimental Setup

Datasets. For outdoor scenarios, we evaluate our method on the KITTI dataset [15]. Following the protocol established in [1, 5, 48], we select 555 point cloud pairs from sequences 8 to 10 for testing. For indoor environments, we conduct experiments on the 3DMatch dataset [45] and the more challenging 3DLoMatch dataset [17], where point cloud pairs have less than 30% overlap. To further assess the robustness and generalization capability of our approach, we also perform experiments on the Bunny model from the Stanford 3D Scanning Repository [10].

Evaluation Criteria. We use rotation error (RE), translation error (TE), and registration recall (RR) as the main evaluation metrics. Following [4, 39, 48], registration is considered successful if the results on the 3DMatch and 3DLoMatch datasets satisfy $RE \leq 15^\circ$ and $TE \leq 30\text{cm}$, or on the KITTI dataset $RE \leq 5^\circ$ and $TE \leq 60\text{cm}$. The mean rotation error and mean translation error are computed only on successfully registered pairs. The registration accuracy of a dataset is defined as the ratio of successfully registered pairs to the total number of pairs.

Implementation details. Our method is implemented in PyTorch. For the 3DMatch, 3DLoMatch, and KITTI datasets, we use Fast Point Feature Histograms (FPFH) [31] and Fully Convolutional Geometric Features (FCGF) [8] as descriptors to generate initial correspondences. Following [4, 39, 21], the Bunny model is downsampled to N_c points and resized to fit a $[0, 1]^3$ cube, creating the source point cloud \mathcal{P} . To generate the target point cloud \mathcal{Q} , a random transformation (\mathbf{R}, \mathbf{t}) is applied to \mathcal{P} and then Gaussian noise $\epsilon_i \sim \mathcal{N}(0, \sigma^2 \mathbf{I}_3)$ is added. A pair of the original and moved points defines an inlier. The inliers are contaminated with outliers generated by random transformations. Detailed computational complexity analysis is provided in the Appendix A.3. All experiments are conducted on an AMD Ryzen 9 5950X CPU and a single NVIDIA RTX 3090 GPU.

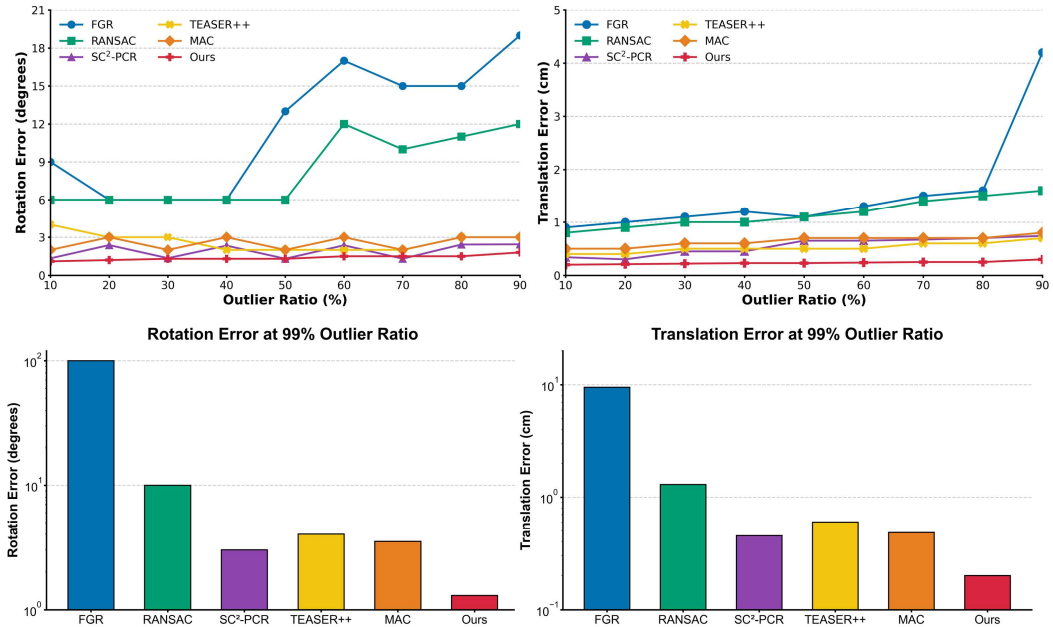


Figure 3: **Outlier robustness evaluation on the synthetic dataset.** The first row shows the rotation and translation errors of each method as the outlier ratio on the Bunny model increases from 10% to 90%. The second row compares the rotation and translation errors of different methods at an outlier ratio of 99%.

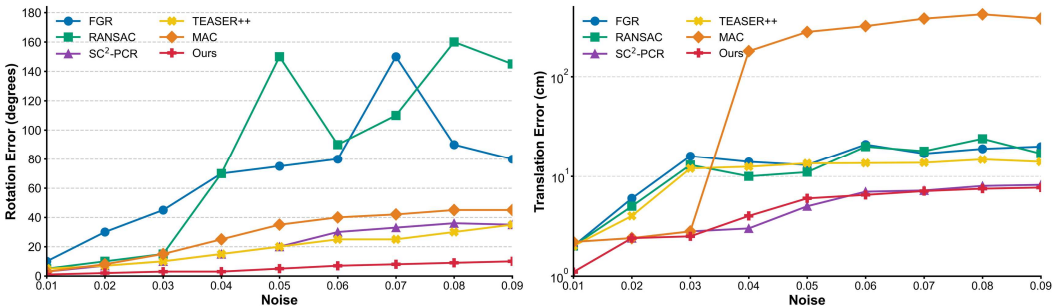


Figure 4: **Noise robustness evaluation on the synthetic dataset.** Comparison of rotation and translation errors on the Bunny model as the noise standard deviation increases from 0.01 to 0.09.

4.2 Robustness to Outliers and Noise on Synthetic Data

On the synthetic dataset, we conduct experiments using the Bunny model. The outlier ratio is varied from 10% to 90% to systematically evaluate the robustness of each method under high outlier rates. The Bunny model is downsampled to $N_c = 500$ and Gaussian noise with zero mean and standard deviation $\sigma = 0.01$ is added. For each outlier ratio, 100 independent trials are performed, and the mean rotation error (RE) and translation error (TE) are recorded. We also test an extreme case with an outlier ratio of up to 99% (please see Fig. 3, second row). Our method is compared against state-of-the-art traditional approaches [51, 14, 5, 39, 48]. Results show that traditional methods such as FGR and RANSAC exhibit rapidly increasing errors as the outlier ratio rises, while our method consistently achieves the best robustness and registration accuracy across all outlier levels.

Table 1: Results on KITTI dataset [15] using FPFH [31] and FCGF [8] descriptors.

	FPFH			FCGF			Time(s)
	RR(%) \uparrow	RE($^{\circ}$) \downarrow	TE(cm) \downarrow	RR(%) \uparrow	RE($^{\circ}$) \downarrow	TE(cm) \downarrow	
<i>i) Traditional</i>							
FGR [51]	5.23	0.86	43.84	89.54	0.46	25.72	3.88
RANSAC [14]	74.41	1.55	30.20	80.36	0.73	26.79	5.43
TEASER++ [39]	91.17	1.03	17.98	95.51	0.33	22.38	0.03
SC ² -PCR [5]	99.46	0.35	7.87	98.02	0.33	20.69	0.31
MAC [48]	97.66	0.41	8.61	97.84	0.34	19.34	3.29
TR-DE [4]	96.76	0.90	15.63	98.20	0.38	18.00	-
TEAR [18]	99.10	0.39	8.62	-	-	-	-
Jiang et al. [21]	99.56	0.34	7.85	98.20	0.32	20.73	0.54
<i>ii) Deep learned</i>							
DGR [7]	77.12	1.64	33.10	96.90	0.34	21.70	2.29
PointDSC [1]	98.92	0.38	8.35	97.84	0.33	20.32	0.45
VBReg [20]	98.92	0.45	8.41	98.02	0.32	20.91	0.24
Ours	99.64	0.43	5.31	99.10	0.59	11.06	0.21

We further evaluate the robustness of each method under different noise levels, as shown in Fig. 4. Specifically, we increase the standard deviation of Gaussian noise from $\sigma = 0.01$ to $\sigma = 0.1$ to systematically assess algorithm performance. Experimental results indicate that, as the noise level increases, the translation error of the clique-based MAC [48] method rises significantly, while our triangle-based method is barely affected. The bundled structure of triangles effectively captures the key skeleton of the point cloud and resists noise interference. As a result, our method consistently achieves the lowest rotation and translation errors under high noise conditions, demonstrating superior robustness.

Table 2: Comparison results on 3DMatch [45] using FPFH [31] and FCGF [8] descriptors.

	FPFH			FCGF			Time(s)
	RR(%) \uparrow	RE($^{\circ}$) \downarrow	TE(cm) \downarrow	RR(%) \uparrow	RE($^{\circ}$) \downarrow	TE(cm) \downarrow	
<i>i) Traditional</i>							
FGR [51]	40.91	4.96	10.25	78.93	2.90	8.41	0.89
RANSAC [14]	66.10	3.95	11.03	91.44	2.69	8.38	2.86
TEASER++ [39]	75.48	2.48	7.31	85.71	2.73	8.66	0.03
SC ² -PCR [5]	83.90	2.12	6.69	93.16	2.06	6.53	0.12
MAC [48]	83.90	<u>2.11</u>	6.80	<u>93.72</u>	2.07	6.52	5.54
FastMAC [49]	82.87	2.15	6.73	92.67	2.00	<u>6.47</u>	0.11
Jiang et al. [21]	<u>83.92</u>	2.12	6.64	93.28	2.04	6.48	0.36
<i>ii) Deep learned</i>							
DGR [7]	32.84	2.45	7.53	88.85	2.28	7.02	1.53
PointDSC [1]	72.95	2.18	<u>6.45</u>	91.87	2.10	6.54	0.10
VBReg [20]	82.57	2.14	6.77	93.53	2.04	6.49	0.20
Ours	84.70	1.80	6.22	93.84	1.70	6.13	0.20

4.3 Experimental Results on the KITTI Dataset

We conduct experiments on the KITTI dataset [15] to evaluate the potential of our algorithm in real outdoor scenarios. Table 1 presents the results using FPFH [31] and FCGF [8] descriptors for initial correspondence generation. We compare our method with leading traditional [51, 14, 39, 5, 48, 4, 18, 21] and learning-based approaches [7, 1, 20]. Following [5, 48], the mean rotation error (RE) and mean translation error (TE) are calculated only on successfully registered pairs. As shown in Table 1, our method achieves the highest recall (RR) and lowest TE with both FPFH and FCGF descriptors. Moreover, our method demonstrates superior efficiency at comparable registration accuracy. These results confirm the robustness of our method for registering sparse and non-uniform outdoor point clouds. Additional visualizations are provided in the Appendix A.10.

Table 3: Comparison results on 3DLoMatch [17] using FPFH [31] and FCGF [8] descriptors.

	FPFH			FCGF		
	RR(%)↑	RE(°)↓	TE(cm)↓	RR(%)↑	RE(°)↓	TE(cm)↓
<i>i) Traditional</i>						
RANSAC [14]	19.83	4.67	10.32	37.60	4.28	11.04
TEASER++ [39]	35.15	4.38	10.96	46.76	4.12	12.89
SC ² -PCR [5]	35.93	4.26	10.86	58.73	3.80	10.44
MAC [48]	<u>40.88</u>	<u>3.66</u>	<u>9.45</u>	<u>59.85</u>	<u>3.50</u>	<u>9.75</u>
FastMAC [49]	38.46	4.04	10.47	58.23	3.80	10.81
<i>ii) Deep learned</i>						
PointDSC [1]	27.91	4.27	10.45	56.20	3.87	10.48
VBReg [20]	30.83	4.38	10.92	58.30	3.58	9.72
Ours	43.96	2.89	8.93	61.64	3.30	9.72

4.4 Experimental Results on the 3DMatch and 3DLoMatch Datasets

We conducted systematic comparative experiments on the 3DMatch dataset with overlap ratios exceeding 30%. The left and right columns of Table 2 show the registration performance using FPFH and FCGF descriptors, respectively. With the handcrafted FPFH descriptor, our method achieves the highest recall (RR), outperforming both traditional and learning-based approaches. Using the FCGF descriptor, our method surpasses all state-of-the-art baselines on every evaluation metric. Compared to the MAC method, our method improves RR by 0.56%. More importantly, it reduces the average rotation error (RE) and average translation error (TE) by about 16.7% and 5.4%, respectively. This demonstrates superior overall performance. Qualitative results are shown in Fig. 5 and Appendix A.10. Our method remains robust even in challenging scenarios with ambiguous features or unclear local structures. It achieves alignment results that are close to the ground truth. These findings strongly validate the robustness and generalization ability of our method on diverse and complex point cloud data.

As shown in Table 3, we systematically evaluated our algorithm on the 3DLoMatch dataset for low-overlap registration. We compared our method with several leading traditional and deep learning approaches, using both FPFH and FCGF descriptors. Our method consistently delivers superior recall rates and reduced error metrics, validating its exceptional robustness and versatility even in challenging low-overlap scenarios. Qualitative results in Fig. 5 and Appendix A.10 further illustrate that our method remains effective even when local structures are ambiguous.

4.5 PointTruss Integration with Deep Learning Methods on 3DLoMatch

We have conducted experiments combining PointTruss with recent deep learning methods [29, 41] on the challenging 3DLoMatch dataset.

PointTruss successfully enhances both GeoTransformer (+4.5% recall) and PareNet (+1.70% recall) on the challenging 3DLoMatch dataset. The consistent improvements across different learned features validate PointTruss’s compatibility with modern deep learning pipelines. Moreover, when integrated with GeoTransformer, PointTruss achieves performance comparable to MAC while being more computationally efficient. These results demonstrate that PointTruss not only works as a standalone

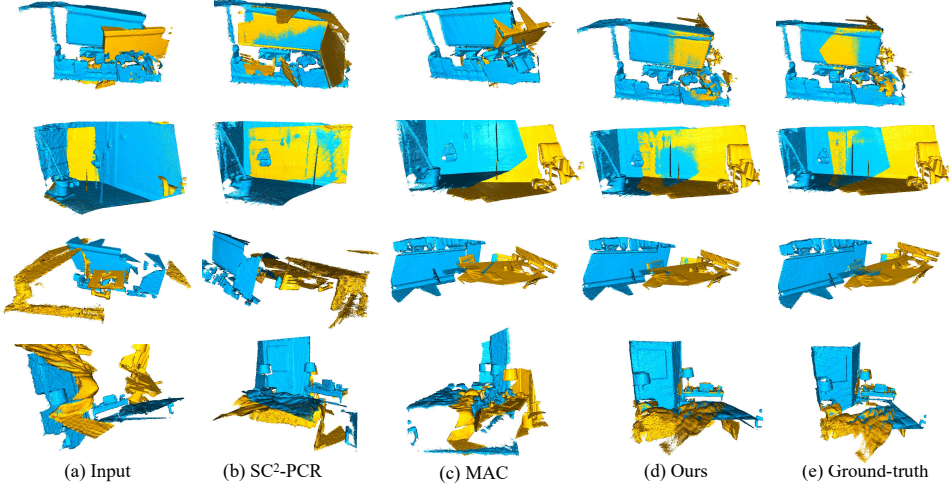


Figure 5: **Qualitative comparisons on the 3DMatch and 3DLoMatch datasets.** The first and second rows correspond to 3DMatch, and the third and fourth rows correspond to 3DLoMatch.

Table 4: PointTruss Integration with Deep Learning Methods on 3DLoMatch

Method	Registration Recall
GeoTransformer	75.0%
GeoTransformer + MAC	78.9%
GeoTransformer + PointTruss	79.5%
PareNet	80.5%
PareNet + MAC	81.5%
PareNet + PointTruss	82.2%

method but also serves as an effective drop-in replacement for traditional robust estimators in deep learning pipelines, providing consistent improvements across different feature extractors.

5 Conclusion

In this work, we introduce the k -truss from graph theory to the point cloud registration and use triangle support as a key constraint. We first perform consensus voting-based low-scale sampling on the input correspondences to construct a compatibility graph. Based on this, we propose a heuristic method that applies k -truss decomposition with triangle support constraints to obtain several k -truss subgraphs. Each candidate subgraph is then processed by weighted SVD, and we use a designed spatial distribution score to evaluate the spatial coverage and uniformity of inliers, selecting the best transformation hypothesis. Our method is efficient and simple, leveraging triangles as minimal rigid planar structures and exploiting their strong structural binding. Experimental results on indoor, outdoor, and object-level point clouds show that our algorithm achieves state-of-the-art registration accuracy while maintaining high efficiency. The method is robust to large numbers of outliers and low-overlap scenarios. Limitations and broader impacts are discussed in Appendix A.7.

6 Acknowledgements

This work is supported by the National Natural Science Foundation of China (62036006, 62276200) and the Innovation Capability Support Plan of Shaanxi Province (2023KJXX-144).

References

- [1] Xuyang Bai, Zixin Luo, Lei Zhou, Hongkai Chen, Lei Li, et al. PointDSC: Robust point cloud registration using deep spatial consistency. In *Proceedings of the IEEE Conference on Computer Vision and Pattern Recognition*, pages 15859–15869, 2021.
- [2] Daniel Barath and Jiří Matas. Graph-Cut RANSAC. In *Proceedings of the IEEE Conference on Computer Vision and Pattern Recognition*, pages 6733–6741, 2018.
- [3] Alvaro Parra Bustos and TatJun Chin. Guaranteed outlier removal for point cloud registration with correspondences. *IEEE Transactions on Pattern Analysis and Machine intelligence*, pages 2868–2882, 2017.
- [4] Wen Chen, Haoang Li, Qiang Nie, and YunHui Liu. Deterministic point cloud registration via novel transformation decomposition. In *Proceedings of the IEEE Conference on Computer Vision and Pattern Recognition*, pages 6348–6356, 2022.
- [5] Zhi Chen, Kun Sun, Fan Yang, and Wenbing Tao. SC2-PCR: A second order spatial compatibility for efficient and robust point cloud registration. In *Proceedings of the IEEE Conference on Computer Vision and Pattern Recognition*, pages 13221–13231, 2022.
- [6] YenChi Cheng, HsinYing Lee, Sergey Tulyakov, Alexander G Schwing, and LiangYan Gui. SDFusion: Multimodal 3D shape completion, reconstruction, and generation. In *Proceedings of the IEEE Conference on Computer Vision and Pattern Recognition*, pages 4456–4465, 2023.
- [7] Christopher Choy, Wei Dong, and Vladlen Koltun. Deep global registration. In *Proceedings of the IEEE Conference on Computer Vision and Pattern Recognition*, pages 2514–2523, 2020.
- [8] Christopher Choy, Jaesik Park, and Vladlen Koltun. Fully convolutional geometric features. In *Proceedings of the IEEE Conference on Computer Vision and Pattern Recognition*, pages 8958–8966, 2019.
- [9] Jonathan Cohen. Trusses: Cohesive subgraphs for social network analysis. *National security agency technical report*, pages 1–29, 2008.
- [10] Brian Curless and Marc Levoy. A volumetric method for building complex models from range images. In *Proceedings of the 23rd annual conference on Computer graphics and interactive techniques*, pages 303–312, 1996.
- [11] Angela Dai, Matthias Nießner, Michael Zollhöfer, Shahram Izadi, and Christian Theobalt. Bundlefusion: Real-time globally consistent 3D reconstruction using on-the-fly surface reintegration. *ACM Transactions on Graphics*, page 1, 2017.
- [12] Dexin Duan, Peilin Liu, Bingwei Hui, and Fei Wen. Brain-inspired online adaptation for remote sensing with spiking neural network. *IEEE Transactions on Geoscience and Remote Sensing*, 2025.
- [13] David Eppstein, Maarten Löffler, and Darren Strash. Listing all maximal cliques in sparse graphs in near-optimal time. In *Algorithms and Computation: 21st International Symposium*, pages 403–414. Springer, 2010.
- [14] Martin A Fischler and Robert C Bolles. Random sample consensus: a paradigm for model fitting with applications to image analysis and automated cartography. *Communications of the ACM*, pages 381–395, 1981.
- [15] Andreas Geiger, Philip Lenz, and Raquel Urtasun. Are we ready for autonomous driving? the kitti vision benchmark suite. In *Proceedings of the IEEE Conference on Computer Vision and Pattern Recognition*, pages 3354–3361, 2012.
- [16] Maciej Halber and Thomas Funkhouser. Fine-to-coarse global registration of rgb-d scans. In *Proceedings of the IEEE Conference on Computer Vision and Pattern Recognition*, pages 1755–1764, 2017.
- [17] Shengyu Huang, Zan Gojcic, Mikhail Usvyatsov, Andreas Wieser, and Konrad Schindler. Predator: Registration of 3D point clouds with low overlap. In *Proceedings of the IEEE Conference on Computer Vision and Pattern Recognition*, pages 4267–4276, 2021.
- [18] Tianyu Huang, Liangzu Peng, René Vidal, and Yun-Hui Liu. Scalable 3D registration via truncated entry-wise absolute residuals. In *Proceedings of the IEEE Conference on Computer Vision and Pattern Recognition*, pages 27477–27487, 2024.
- [19] Xiaoshui Huang, Guofeng Mei, Jian Zhang, and Rana Abbas. A comprehensive survey on point cloud registration. *arXiv preprint arXiv:2103.02690*, 2021.

[20] Haobo Jiang, Zheng Dang, Zhen Wei, Jin Xie, Jian Yang, and Mathieu Salzmann. Robust outlier rejection for 3D registration with variational bayes. In *Proceedings of the IEEE Conference on Computer Vision and Pattern Recognition*, pages 1148–1157, 2023.

[21] Yinuo Jiang, Xiuchuan Tang, Cheng Cheng, and Ye Yuan. A robust inlier identification algorithm for point cloud registration via ℓ_0 -minimization. *Advances in Neural Information Processing Systems*, pages 63124–63153, 2024.

[22] Kevin Lai, Liefeng Bo, and Dieter Fox. Unsupervised feature learning for 3D scene labeling. In *IEEE International Conference on Robotics and Automation*, pages 3050–3057, 2014.

[23] Junha Lee, Seungwook Kim, Minsu Cho, and Jaesik Park. Deep hough voting for robust global registration. In *Proceedings of the IEEE Conference on Computer Vision and Pattern Recognition*, pages 15994–16003, 2021.

[24] Marius Leordeanu and Martial Hebert. A spectral technique for correspondence problems using pairwise constraints. In *Proceedings of the IEEE International Conference on Computer Vision*, pages 1482–1489. IEEE, 2005.

[25] Jiayuan Li, Pengcheng Shi, Qingwu Hu, and Yongjun Zhang. QGORE: Quadratic-time guaranteed outlier removal for point cloud registration. *IEEE Transactions on Pattern Analysis and Machine Intelligence*, pages 11136–11151, 2023.

[26] Boge Liu, Fan Zhang, Wenjie Zhang, Xuemin Lin, and Ying Zhang. Efficient community search with size constraint. In *IEEE International Conference on Data Engineering*, pages 97–108, 2021.

[27] Alexander Neubeck and Luc Van Gool. Efficient non-maximum suppression. In *Proceedings of the 18th International Conference on Pattern Recognition*, pages 850–855. IEEE, 2006.

[28] Liangzu Peng, Manolis C Tsakiris, and René Vidal. Arcs: Accurate rotation and correspondence search. In *Proceedings of the IEEE Conference on Computer Vision and Pattern Recognition*, pages 11153–11163, 2022.

[29] Zheng Qin, Hao Yu, Changjian Wang, Yulan Guo, Yuxing Peng, Slobodan Ilic, Dewen Hu, and Kai Xu. Geotransformer: Fast and robust point cloud registration with geometric transformer. *IEEE Transactions on Pattern Analysis and Machine Intelligence*, pages 9806–9821, 2023.

[30] Siwen Quan and Jiaqi Yang. Compatibility-guided sampling consensus for 3-D point cloud registration. *IEEE Transactions on Geoscience and Remote Sensing*, pages 7380–7392, 2020.

[31] Radu Bogdan Rusu, Nico Blodow, and Michael Beetz. Fast point feature histograms FPFH for 3D registration. In *IEEE International Conference on Robotics and Automation*, pages 3212–3217, 2009.

[32] Jingnan Shi, Heng Yang, and Luca Carlone. Robin: a graph-theoretic approach to reject outliers in robust estimation using invariants. In *IEEE International Conference on Robotics and Automation*, pages 13820–13827, 2021.

[33] Jamie Shotton, Ben Glocker, Christopher Zach, Shahram Izadi, Antonio Criminisi, and Andrew Fitzgibbon. Scene coordinate regression forests for camera relocalization in rgb-d images. In *Proceedings of the IEEE Conference on Computer Vision and Pattern Recognition*, pages 2930–2937, 2013.

[34] Chitturi Sidhartha, Lalit Manam, and Venu Madhav Govindu. Adaptive annealing for robust geometric estimation. In *Proceedings of the IEEE Conference on Computer Vision and Pattern Recognition*, pages 21929–21939, 2023.

[35] Lei Sun. Suc oft: Robust point cloud registration based on guaranteed supercore maximization and flexible thresholding. *IEEE Transactions on Geoscience and Remote Sensing*, pages 1–21, 2024.

[36] Julien Valentin, Angela Dai, Matthias Nießner, Pushmeet Kohli, Philip Torr, Shahram Izadi, and Cem Keskin. Learning to navigate the energy landscape. In *International Conference on 3D Vision*, pages 323–332, 2016.

[37] Yue Wu, Xidao Hu, Yongzhe Yuan, Xiaolong Fan, Maoguo Gong, Hao Li, Mingyang Zhang, Qiguang Miao, and Wenping Ma. Pointmc: multi-instance point cloud registration based on maximal cliques. In *Proceedings of the 41st International Conference on Machine Learning*, 2024.

[38] Jianxiong Xiao, Andrew Owens, and Antonio Torralba. Sun3d: A database of big spaces reconstructed using sfm and object labels. In *Proceedings of the IEEE Conference on Computer Vision and Pattern Recognition*, pages 1625–1632, 2013.

[39] Heng Yang, Jingnan Shi, and Luca Carlone. Teaser: Fast and certifiable point cloud registration. *IEEE Transactions on Robotics*, pages 314–333, 2020.

[40] Jiaqi Yang, Xiyu Zhang, Shichao Fan, Chunlin Ren, and Yanning Zhang. Mutual voting for ranking 3d correspondences. *IEEE Transactions on Pattern Analysis and Machine Intelligence*, pages 4041–4057, 2023.

[41] Runzhao Yao, Shaoyi Du, Wenting Cui, Canhui Tang, and Chengwu Yang. Pare-net: Position-aware rotation-equivariant networks for robust point cloud registration. In *European Conference on Computer Vision*, pages 287–303. Springer, 2024.

[42] Yongzhe Yuan, Yue Wu, Xiaolong Fan, Maoguo Gong, Wenping Ma, et al. EGST: Enhanced geometric structure transformer for point cloud registration. *IEEE Transactions on Visualization and Computer Graphics*, 2023. doi:10.1109/TVCG.2023.3329578.

[43] Yongzhe Yuan, Yue Wu, Xiaolong Fan, Maoguo Gong, Qiguang Miao, and Wenping Ma. Inlier confidence calibration for point cloud registration. In *Proceedings of the IEEE Conference on Computer Vision and Pattern Recognition*, pages 5312–5321, 2024.

[44] Yongzhe Yuan, Yue Wu, Xiaolong Fan, Maoguo Gong, Qiguang Miao, and Wenping Ma. Where precision meets efficiency: Transformation diffusion model for point cloud registration. In *Proceedings of the AAAI Conference on Artificial Intelligence*, volume 39, pages 9734–9742, 2025.

[45] Andy Zeng, Shuran Song, Matthias Nießner, Matthew Fisher, Jianxiong Xiao, and T Funkhouser. 3Dmatch: Learning the matching of local 3D geometry in range scans. In *Proceedings of the IEEE Conference on Computer Vision and Pattern Recognition*, page 4, 2017.

[46] Fan Zhang, Haicheng Guo, Dian Ouyang, Shiyu Yang, Xuemin Lin, and Zhihong Tian. Size-constrained community search on large networks: An effective and efficient solution. *IEEE Transactions on Knowledge and Data Engineering*, pages 356–371, 2023.

[47] Fan Zhang, Conggai Li, Ying Zhang, Lu Qin, and Wenjie Zhang. Finding critical users in social communities: The collapsed core and truss problems. *IEEE Transactions on Knowledge and Data Engineering*, pages 78–91, 2018.

[48] Xiyu Zhang, Jiaqi Yang, Shikun Zhang, and Yanning Zhang. 3D registration with maximal cliques. In *Proceedings of the IEEE Conference on Computer Vision and Pattern Recognition*, pages 17745–17754, 2023.

[49] Yifei Zhang, Hao Zhao, Hongyang Li, and Siheng Chen. Fastmac: Stochastic spectral sampling of correspondence graph. In *Proceedings of the IEEE Conference on Computer Vision and Pattern Recognition*, pages 17857–17867, 2024.

[50] Haimei Zhao, Jing Zhang, Zhuo Chen, Bo Yuan, and Dacheng Tao. On robust cross-view consistency in self-supervised monocular depth estimation. *Machine Intelligence Research*, pages 495–513, 2024.

[51] QianYi Zhou, Jaesik Park, and Vladlen Koltun. Fast global registration. In *European Conference on Computer Vision*, pages 766–782. Springer, 2016.

NeurIPS Paper Checklist

1. Claims

Question: Do the main claims made in the abstract and introduction accurately reflect the paper's contributions and scope?

Answer: [\[Yes\]](#)

Justification: The claims and contributions of the paper are clearly articulated in the abstract and introduction, and demonstrate good generalizability under similar assumptions.

Guidelines:

- The answer NA means that the abstract and introduction do not include the claims made in the paper.
- The abstract and/or introduction should clearly state the claims made, including the contributions made in the paper and important assumptions and limitations. A No or NA answer to this question will not be perceived well by the reviewers.
- The claims made should match theoretical and experimental results, and reflect how much the results can be expected to generalize to other settings.
- It is fine to include aspirational goals as motivation as long as it is clear that these goals are not attained by the paper.

2. Limitations

Question: Does the paper discuss the limitations of the work performed by the authors?

Answer: [\[Yes\]](#)

Justification: The paper discusses the limitations of the work in Appendix A.7.

Guidelines:

- The answer NA means that the paper has no limitation while the answer No means that the paper has limitations, but those are not discussed in the paper.
- The authors are encouraged to create a separate "Limitations" section in their paper.
- The paper should point out any strong assumptions and how robust the results are to violations of these assumptions (e.g., independence assumptions, noiseless settings, model well-specification, asymptotic approximations only holding locally). The authors should reflect on how these assumptions might be violated in practice and what the implications would be.
- The authors should reflect on the scope of the claims made, e.g., if the method was only tested on a few datasets or with a few runs. In general, empirical results often depend on implicit assumptions, which should be articulated.
- The authors should reflect on the factors that influence the performance of the method. For example, a facial recognition algorithm may perform poorly when image resolution is low or images are taken in low lighting. Or a speech-to-text system might not be used reliably to provide closed captions for online lectures because it fails to handle technical jargon.
- The authors should discuss the computational efficiency of the proposed algorithms and how they scale with dataset size.
- If applicable, the authors should discuss possible limitations of their method to address problems of privacy and fairness.
- While the authors might fear that complete honesty about limitations might be used by reviewers as grounds for rejection, a worse outcome might be that reviewers discover limitations that aren't acknowledged in the paper. The authors should use their best judgment and recognize that individual actions in favor of transparency play an important role in developing norms that preserve the integrity of the community. Reviewers will be specifically instructed to not penalize honesty concerning limitations.

3. Theory assumptions and proofs

Question: For each theoretical result, does the paper provide the full set of assumptions and a complete (and correct) proof?

Answer: [\[Yes\]](#)

Justification: The paper presents theorems and formulas in Sec. 3, and reports theoretical results in Sec. 4. We systematically derive the statistical properties of triangle relations under rigid-body noise and provide a rigorous theoretical foundation for the robust discriminative power of the k -truss. The detailed derivations are presented in Appendix A.2.

Guidelines:

- The answer NA means that the paper does not include theoretical results.
- All the theorems, formulas, and proofs in the paper should be numbered and cross-referenced.
- All assumptions should be clearly stated or referenced in the statement of any theorems.
- The proofs can either appear in the main paper or the supplemental material, but if they appear in the supplemental material, the authors are encouraged to provide a short proof sketch to provide intuition.
- Inversely, any informal proof provided in the core of the paper should be complemented by formal proofs provided in appendix or supplemental material.
- Theorems and Lemmas that the proof relies upon should be properly referenced.

4. Experimental result reproducibility

Question: Does the paper fully disclose all the information needed to reproduce the main experimental results of the paper to the extent that it affects the main claims and/or conclusions of the paper (regardless of whether the code and data are provided or not)?

Answer: [\[Yes\]](#)

Justification: We provide a detailed description of the algorithmic procedure in the paper, and the main experimental results are reproducible. The code will be made publicly available upon acceptance of the paper.

Guidelines:

- The answer NA means that the paper does not include experiments.
- If the paper includes experiments, a No answer to this question will not be perceived well by the reviewers: Making the paper reproducible is important, regardless of whether the code and data are provided or not.
- If the contribution is a dataset and/or model, the authors should describe the steps taken to make their results reproducible or verifiable.
- Depending on the contribution, reproducibility can be accomplished in various ways. For example, if the contribution is a novel architecture, describing the architecture fully might suffice, or if the contribution is a specific model and empirical evaluation, it may be necessary to either make it possible for others to replicate the model with the same dataset, or provide access to the model. In general, releasing code and data is often one good way to accomplish this, but reproducibility can also be provided via detailed instructions for how to replicate the results, access to a hosted model (e.g., in the case of a large language model), releasing of a model checkpoint, or other means that are appropriate to the research performed.
- While NeurIPS does not require releasing code, the conference does require all submissions to provide some reasonable avenue for reproducibility, which may depend on the nature of the contribution. For example
 - (a) If the contribution is primarily a new algorithm, the paper should make it clear how to reproduce that algorithm.
 - (b) If the contribution is primarily a new model architecture, the paper should describe the architecture clearly and fully.
 - (c) If the contribution is a new model (e.g., a large language model), then there should either be a way to access this model for reproducing the results or a way to reproduce the model (e.g., with an open-source dataset or instructions for how to construct the dataset).
 - (d) We recognize that reproducibility may be tricky in some cases, in which case authors are welcome to describe the particular way they provide for reproducibility. In the case of closed-source models, it may be that access to the model is limited in some way (e.g., to registered users), but it should be possible for other researchers to have some path to reproducing or verifying the results.

5. Open access to data and code

Question: Does the paper provide open access to the data and code, with sufficient instructions to faithfully reproduce the main experimental results, as described in supplemental material?

Answer: [No]

Justification: We will make the complete code public following the acceptance of the paper.

Guidelines:

- The answer NA means that paper does not include experiments requiring code.
- Please see the NeurIPS code and data submission guidelines (<https://nips.cc/public/guides/CodeSubmissionPolicy>) for more details.
- While we encourage the release of code and data, we understand that this might not be possible, so “No” is an acceptable answer. Papers cannot be rejected simply for not including code, unless this is central to the contribution (e.g., for a new open-source benchmark).
- The instructions should contain the exact command and environment needed to run to reproduce the results. See the NeurIPS code and data submission guidelines (<https://nips.cc/public/guides/CodeSubmissionPolicy>) for more details.
- The authors should provide instructions on data access and preparation, including how to access the raw data, preprocessed data, intermediate data, and generated data, etc.
- The authors should provide scripts to reproduce all experimental results for the new proposed method and baselines. If only a subset of experiments are reproducible, they should state which ones are omitted from the script and why.
- At submission time, to preserve anonymity, the authors should release anonymized versions (if applicable).
- Providing as much information as possible in supplemental material (appended to the paper) is recommended, but including URLs to data and code is permitted.

6. Experimental setting/details

Question: Does the paper specify all the training and test details (e.g., data splits, hyper-parameters, how they were chosen, type of optimizer, etc.) necessary to understand the results?

Answer: [Yes]

Justification: The experimental setup and implement details are provided in Sec. 4.1, as well as in Appendix A.5.

Guidelines:

- The answer NA means that the paper does not include experiments.
- The experimental setting should be presented in the core of the paper to a level of detail that is necessary to appreciate the results and make sense of them.
- The full details can be provided either with the code, in appendix, or as supplemental material.

7. Experiment statistical significance

Question: Does the paper report error bars suitably and correctly defined or other appropriate information about the statistical significance of the experiments?

Answer: [Yes]

Justification: We conducted multiple experiments on public datasets as described in Sec. 4. Furthermore, we performed 100 independent runs in Sec. 4.2, and the averaged results demonstrate that our experimental outcomes are stable across multiple runs.

Guidelines:

- The answer NA means that the paper does not include experiments.
- The authors should answer “Yes” if the results are accompanied by error bars, confidence intervals, or statistical significance tests, at least for the experiments that support the main claims of the paper.

- The factors of variability that the error bars are capturing should be clearly stated (for example, train/test split, initialization, random drawing of some parameter, or overall run with given experimental conditions).
- The method for calculating the error bars should be explained (closed form formula, call to a library function, bootstrap, etc.)
- The assumptions made should be given (e.g., Normally distributed errors).
- It should be clear whether the error bar is the standard deviation or the standard error of the mean.
- It is OK to report 1-sigma error bars, but one should state it. The authors should preferably report a 2-sigma error bar than state that they have a 96% CI, if the hypothesis of Normality of errors is not verified.
- For asymmetric distributions, the authors should be careful not to show in tables or figures symmetric error bars that would yield results that are out of range (e.g. negative error rates).
- If error bars are reported in tables or plots, The authors should explain in the text how they were calculated and reference the corresponding figures or tables in the text.

8. Experiments compute resources

Question: For each experiment, does the paper provide sufficient information on the computer resources (type of compute workers, memory, time of execution) needed to reproduce the experiments?

Answer: [\[Yes\]](#)

Justification: We provide information on the compute workers and model efficiency in Sec. 4.1, Sec. 4.3 and Sec. 4.4.

Guidelines:

- The answer NA means that the paper does not include experiments.
- The paper should indicate the type of compute workers CPU or GPU, internal cluster, or cloud provider, including relevant memory and storage.
- The paper should provide the amount of compute required for each of the individual experimental runs as well as estimate the total compute.
- The paper should disclose whether the full research project required more compute than the experiments reported in the paper (e.g., preliminary or failed experiments that didn't make it into the paper).

9. Code of ethics

Question: Does the research conducted in the paper conform, in every respect, with the NeurIPS Code of Ethics <https://neurips.cc/public/EthicsGuidelines>?

Answer: [\[Yes\]](#)

Justification: This article complies in all respects with the NeurIPS Code of Ethics.

Guidelines:

- The answer NA means that the authors have not reviewed the NeurIPS Code of Ethics.
- If the authors answer No, they should explain the special circumstances that require a deviation from the Code of Ethics.
- The authors should make sure to preserve anonymity (e.g., if there is a special consideration due to laws or regulations in their jurisdiction).

10. Broader impacts

Question: Does the paper discuss both potential positive societal impacts and negative societal impacts of the work performed?

Answer: [\[Yes\]](#)

Justification: The potential positive and negative societal impacts of the work are discussed in Appendix A.7.

Guidelines:

- The answer NA means that there is no societal impact of the work performed.

- If the authors answer NA or No, they should explain why their work has no societal impact or why the paper does not address societal impact.
- Examples of negative societal impacts include potential malicious or unintended uses (e.g., disinformation, generating fake profiles, surveillance), fairness considerations (e.g., deployment of technologies that could make decisions that unfairly impact specific groups), privacy considerations, and security considerations.
- The conference expects that many papers will be foundational research and not tied to particular applications, let alone deployments. However, if there is a direct path to any negative applications, the authors should point it out. For example, it is legitimate to point out that an improvement in the quality of generative models could be used to generate deepfakes for disinformation. On the other hand, it is not needed to point out that a generic algorithm for optimizing neural networks could enable people to train models that generate Deepfakes faster.
- The authors should consider possible harms that could arise when the technology is being used as intended and functioning correctly, harms that could arise when the technology is being used as intended but gives incorrect results, and harms following from (intentional or unintentional) misuse of the technology.
- If there are negative societal impacts, the authors could also discuss possible mitigation strategies (e.g., gated release of models, providing defenses in addition to attacks, mechanisms for monitoring misuse, mechanisms to monitor how a system learns from feedback over time, improving the efficiency and accessibility of ML).

11. Safeguards

Question: Does the paper describe safeguards that have been put in place for responsible release of data or models that have a high risk for misuse (e.g., pretrained language models, image generators, or scraped datasets)?

Answer: [NA]

Justification: The paper poses no such risks.

Guidelines:

- The answer NA means that the paper poses no such risks.
- Released models that have a high risk for misuse or dual-use should be released with necessary safeguards to allow for controlled use of the model, for example by requiring that users adhere to usage guidelines or restrictions to access the model or implementing safety filters.
- Datasets that have been scraped from the Internet could pose safety risks. The authors should describe how they avoided releasing unsafe images.
- We recognize that providing effective safeguards is challenging, and many papers do not require this, but we encourage authors to take this into account and make a best faith effort.

12. Licenses for existing assets

Question: Are the creators or original owners of assets (e.g., code, data, models), used in the paper, properly credited and are the license and terms of use explicitly mentioned and properly respected?

Answer: [Yes]

Justification: The paper uses publicly available code and datasets during the evaluation process, strictly adhering to all relevant protocols and usage restrictions. Detailed license information for each dataset is provided in Appendix A.9.

Guidelines:

- The answer NA means that the paper does not use existing assets.
- The authors should cite the original paper that produced the code package or dataset.
- The authors should state which version of the asset is used and, if possible, include a URL.
- The name of the license (e.g., CC-BY 4.0) should be included for each asset.

- For scraped data from a particular source (e.g., website), the copyright and terms of service of that source should be provided.
- If assets are released, the license, copyright information, and terms of use in the package should be provided. For popular datasets, paperswithcode.com/datasets has curated licenses for some datasets. Their licensing guide can help determine the license of a dataset.
- For existing datasets that are re-packaged, both the original license and the license of the derived asset (if it has changed) should be provided.
- If this information is not available online, the authors are encouraged to reach out to the asset's creators.

13. New assets

Question: Are new assets introduced in the paper well documented and is the documentation provided alongside the assets?

Answer: [NA]

Justification: We will release the our code under the CC BY-NC-SA 4.0 license after the acceptance of the paper.

Guidelines:

- The answer NA means that the paper does not release new assets.
- Researchers should communicate the details of the dataset/code/model as part of their submissions via structured templates. This includes details about training, license, limitations, etc.
- The paper should discuss whether and how consent was obtained from people whose asset is used.
- At submission time, remember to anonymize your assets (if applicable). You can either create an anonymized URL or include an anonymized zip file.

14. Crowdsourcing and research with human subjects

Question: For crowdsourcing experiments and research with human subjects, does the paper include the full text of instructions given to participants and screenshots, if applicable, as well as details about compensation (if any)?

Answer: [NA]

Justification: The paper does not involve crowdsourcing nor research with human subjects.

Guidelines:

- The answer NA means that the paper does not involve crowdsourcing nor research with human subjects.
- Including this information in the supplemental material is fine, but if the main contribution of the paper involves human subjects, then as much detail as possible should be included in the main paper.
- According to the NeurIPS Code of Ethics, workers involved in data collection, curation, or other labor should be paid at least the minimum wage in the country of the data collector.

15. Institutional review board (IRB) approvals or equivalent for research with human subjects

Question: Does the paper describe potential risks incurred by study participants, whether such risks were disclosed to the subjects, and whether Institutional Review Board (IRB) approvals (or an equivalent approval/review based on the requirements of your country or institution) were obtained?

Answer: [NA]

Justification: The paper does not involve crowdsourcing nor research with human subjects.

Guidelines:

- The answer NA means that the paper does not involve crowdsourcing nor research with human subjects.

- Depending on the country in which research is conducted, IRB approval (or equivalent) may be required for any human subjects research. If you obtained IRB approval, you should clearly state this in the paper.
- We recognize that the procedures for this may vary significantly between institutions and locations, and we expect authors to adhere to the NeurIPS Code of Ethics and the guidelines for their institution.
- For initial submissions, do not include any information that would break anonymity (if applicable), such as the institution conducting the review.

16. Declaration of LLM usage

Question: Does the paper describe the usage of LLMs if it is an important, original, or non-standard component of the core methods in this research? Note that if the LLM is used only for writing, editing, or formatting purposes and does not impact the core methodology, scientific rigorousness, or originality of the research, declaration is not required.

Answer: [NA]

Justification: In this paper, LLMs are not used as any important, original, or non-standard component.

Guidelines:

- The answer NA means that the core method development in this research does not involve LLMs as any important, original, or non-standard components.
- Please refer to our LLM policy (<https://neurips.cc/Conferences/2025/LLM>) for what should or should not be described.

A Appendix

In the appendix, we first provide rigorous definitions of evaluation metrics (Sec. A.1). We then present the Triangle Relation Stability Theorem for point cloud registration (Sec. A.2). A computational complexity analysis and comparison of dense subgraph algorithms is given in Sec. A.3. We further describe pseudocode for key algorithmic components (Sec. A.4) and provide specific hyper-parameter selections for reference (Sec. A.5). Additionally, we conduct ablation studies of each component (Sec. A.6) and discuss the limitations and scalability of our method (Sec. A.7 and Sec. A.8). We offer detailed information on public datasets (Sec. A.9) along with their visualization results (Sec. A.10). We also present an ablation study on graph sampling and the k -value (Sec. A.11).

A.1 The rigorous definitions of Evaluation Metrics

Rotation Error (RE) For a given point cloud pair, the rotation error measures the angular difference between the estimated rotation \mathbf{R} and the ground truth rotation \mathbf{R}_{gt} , computed as:

$$RE = \arccos \frac{\text{trace}(\mathbf{R}_{gt}\mathbf{R}^T) - 1}{2} \quad (18)$$

Translation Error (TE) The translation error measures the Euclidean distance between the estimated translation \mathbf{t} and the ground truth translation \mathbf{t}_{gt} :

$$TE = \|\mathbf{t} - \mathbf{t}_{gt}\|_2 \quad (19)$$

Registration Recall (RR) Registration recall measures the percentage of successfully registered point cloud pairs over all pairs in the dataset. A registration is considered successful if:

$$RR_{3DMatch\&3DLoMatch} = \frac{1}{N} \sum_{i=1}^N [RE_i < 15^\circ \wedge TE_i < 30 \text{ cm}] \quad (20)$$

$$RR_{KITTI} = \frac{1}{N} \sum_{i=1}^N [RE_i < 5^\circ \wedge TE_i < 60 \text{ cm}] \quad (21)$$

Mean Rotation and Translation Errors The mean rotation and translation errors are computed only over the successfully registered point cloud pairs:

$$\text{Mean RE} = \frac{1}{|N'|} \sum_{i \in N'} RE_i \quad (22)$$

$$\text{Mean TE} = \frac{1}{|N'|} \sum_{i \in N'} TE_i \quad (23)$$

where $N' = \{i \mid RE_i < \tau_{RE} \wedge TE_i < \tau_{TE}\}$ denotes the set of successfully registered pairs, with $\tau_{RE} = 15^\circ$ and $\tau_{TE} = 30 \text{ cm}$ for 3DMatch and 3DLoMatch, and $\tau_{RE} = 5^\circ$ and $\tau_{TE} = 60 \text{ cm}$ for KITTI.

A.2 Triangle Relation Stability Theorem Based Point Cloud Registration

The PointTruss registration framework introduces a novel perspective by leveraging the k -truss from graph theory to establish robust correspondence patterns in point cloud registration. At the core of k -truss lies the concept of triangle support—each edge in a k -truss is contained in at least $k-2$ triangles, providing exceptional structural stability against perturbations. This property is particularly advantageous in point cloud registration, where noise, outliers, and partial visibility are common challenges.

Before developing the algorithmic components of PointTruss, it is essential to establish a rigorous theoretical foundation that quantifies how triangle relations behave under noise and rigid transformations. Specifically, we need to mathematically prove why triangle relations remain stable for

correct correspondences while exhibiting significant deviations for incorrect ones. This theoretical foundation addresses several critical questions:

1. How do triangle relations (edge lengths) change under noise perturbation?
2. What statistical properties characterize these changes?
3. Under what conditions can we reliably distinguish between correct and incorrect point correspondences based on triangle relation stability?
4. Why does the triangle-supported k -truss provide a reliable foundation for robust registration?

The following theorem establishes the statistical properties of triangle relations under noise, providing the theoretical underpinning for the PointTruss registration framework. By demonstrating that correct correspondences maintain stable triangle relations with high probability, this analysis justifies using triangle-based constraints as a core mechanism for robust point cloud registration.

Let $\mathcal{P} = \{p_i\}_{i=1}^N$ denote the source point cloud and $\mathcal{Q} = \{q_i\}_{i=1}^N$ denote the target point cloud after rigid transformation and noise perturbation, where $p_i, q_i \in \mathbb{R}^3$. The rigid transformation is defined as $T = (R, t)$, where $R \in SO(3)$ is a rotation matrix satisfying $R^\top R = I$ and $\det(R) = 1$, and $t \in \mathbb{R}^3$ is a translation vector.

The noise-contaminated point cloud model can be expressed as:

$$q_i = Rp_i + t + \eta_i, \quad \eta_i \sim \mathcal{N}(0, \sigma^2 I) \quad (24)$$

where η_i represents independent and identically distributed Gaussian noise with zero mean and covariance matrix $\sigma^2 I$.

For any pair of points p_i and p_j in the source point cloud, their Euclidean distance is preserved under rigid transformation. Let $d_{ij} = \|p_i - p_j\|$ denote the distance between points p_i and p_j . In the absence of noise, the distance between the corresponding transformed points q_i and q_j is:

$$\begin{aligned} \|q_i - q_j\| &= \|Rp_i + t - (Rp_j + t)\| \\ &= \|R(p_i - p_j)\| \\ &= \sqrt{(R(p_i - p_j))^\top (R(p_i - p_j))} \\ &= \sqrt{(p_i - p_j)^\top R^\top R(p_i - p_j)} \\ &= \sqrt{(p_i - p_j)^\top I(p_i - p_j)} \\ &= \|p_i - p_j\| = d_{ij} \end{aligned} \quad (25)$$

This distance preservation property is a fundamental characteristic of rigid transformations.

For any triplet of points (p_i, p_j, p_k) in the source point cloud, we define the triangle relation matrix D_{ijk} as:

$$D_{ijk} = [\|p_i - p_j\| \quad \|p_i - p_k\| \quad \|p_j - p_k\|] \quad (26)$$

Similarly, for the corresponding points in the target point cloud, the triangle relation matrix is:

$$D'_{ijk} = [\|q_i - q_j\| \quad \|q_i - q_k\| \quad \|q_j - q_k\|] \quad (27)$$

Under noise-free rigid transformation, $D_{ijk} = D'_{ijk}$, reflecting the invariance of triangle relations under rigid transformations.

In the presence of noise, the distance between two points in the target point cloud becomes:

$$\begin{aligned}
\|q_i - q_j\| &= \|Rp_i + t + \eta_i - (Rp_j + t + \eta_j)\| \\
&= \|R(p_i - p_j) + (\eta_i - \eta_j)\| \\
&= \|p_i - p_j + R^\top(\eta_i - \eta_j)\| \\
&= \|p_i - p_j + Z_{ij}\|
\end{aligned} \tag{28}$$

where $Z_{ij} = R^\top(\eta_i - \eta_j) \sim \mathcal{N}(0, 2\sigma^2 I)$ represents the transformed noise difference.

The squared distance between noisy points can be expanded as:

$$\begin{aligned}
\|q_i - q_j\|^2 &= \|p_i - p_j + Z_{ij}\|^2 \\
&= (p_i - p_j + Z_{ij})^\top (p_i - p_j + Z_{ij}) \\
&= (p_i - p_j)^\top (p_i - p_j) + 2(p_i - p_j)^\top Z_{ij} + Z_{ij}^\top Z_{ij} \\
&= \|p_i - p_j\|^2 + 2(p_i - p_j)^\top Z_{ij} + \|Z_{ij}\|^2
\end{aligned} \tag{29}$$

Taking the expectation:

$$\begin{aligned}
\mathbb{E}[\|q_i - q_j\|^2] &= \mathbb{E}[\|p_i - p_j\|^2 + 2(p_i - p_j)^\top Z_{ij} + \|Z_{ij}\|^2] \\
&= \|p_i - p_j\|^2 + \mathbb{E}[2(p_i - p_j)^\top Z_{ij}] + \mathbb{E}[\|Z_{ij}\|^2]
\end{aligned} \tag{30}$$

Since $\mathbb{E}[Z_{ij}] = 0$, the middle term vanishes:

$$\mathbb{E}[2(p_i - p_j)^\top Z_{ij}] = 2(p_i - p_j)^\top \mathbb{E}[Z_{ij}] = 0 \tag{31}$$

For the third term, $\|Z_{ij}\|^2$ follows a chi-squared distribution with 3 degrees of freedom and scaling factor $2\sigma^2$. The expected value of a chi-squared random variable is its degrees of freedom multiplied by the scaling factor:

$$\mathbb{E}[\|Z_{ij}\|^2] = 3 \cdot 2\sigma^2 = 6\sigma^2 \tag{32}$$

Therefore:

$$\mathbb{E}[\|q_i - q_j\|^2] = d_{ij}^2 + 6\sigma^2 \tag{33}$$

To calculate the expected value of $\|q_i - q_j\|$, we apply a first-order Taylor expansion of $f(x) = \sqrt{x}$ around $x = d_{ij}^2$:

$$\begin{aligned}
f(x) &\approx f(d_{ij}^2) + f'(d_{ij}^2)(x - d_{ij}^2) \\
&= \sqrt{d_{ij}^2} + \frac{1}{2\sqrt{d_{ij}^2}}(x - d_{ij}^2) \\
&= d_{ij} + \frac{1}{2d_{ij}}(x - d_{ij}^2)
\end{aligned} \tag{34}$$

For this approximation to be valid, we require $\sigma \ll d_{ij}$, ensuring that higher-order terms (of order $\frac{\sigma^4}{d_{ij}^3}$ and beyond) remain negligible.

Substituting $x = \|q_i - q_j\|^2$ with $\mathbb{E}[x] = d_{ij}^2 + 6\sigma^2$:

$$\begin{aligned}
\mathbb{E}[\|q_i - q_j\|] &\approx d_{ij} + \frac{1}{2d_{ij}}(\mathbb{E}[\|q_i - q_j\|^2] - d_{ij}^2) \\
&= d_{ij} + \frac{1}{2d_{ij}}(d_{ij}^2 + 6\sigma^2 - d_{ij}^2) \\
&= d_{ij} + \frac{1}{2d_{ij}} \cdot 6\sigma^2 \\
&= d_{ij} + \frac{3\sigma^2}{d_{ij}}
\end{aligned} \tag{35}$$

Defining the distance deviation as $\Delta_{ij} = \|q_i - q_j\| - d_{ij}$, its expected value is:

$$\mathbb{E}[\Delta_{ij}] = \mathbb{E}[\|q_i - q_j\|] - d_{ij} \approx \frac{3\sigma^2}{d_{ij}} \tag{36}$$

For more precise analysis, we decompose the noise vector Z_{ij} into components parallel and perpendicular to the direction vector $u_{ij} = \frac{p_i - p_j}{d_{ij}}$:

$$Z_{ij} = Z_{ij,u}u_{ij} + Z_{ij,\perp} \tag{37}$$

where $Z_{ij,u} = Z_{ij} \cdot u_{ij}$ is the projection of noise along u_{ij} , and $Z_{ij,\perp}$ is the perpendicular component.

Using this decomposition, the distance can be more precisely approximated as:

$$\begin{aligned}
\|q_i - q_j\| &= \|d_{ij}u_{ij} + Z_{ij}\| \\
&= \|d_{ij}u_{ij} + Z_{ij,u}u_{ij} + Z_{ij,\perp}\| \\
&= \|(d_{ij} + Z_{ij,u})u_{ij} + Z_{ij,\perp}\| \\
&\approx (d_{ij} + Z_{ij,u})\sqrt{1 + \frac{\|Z_{ij,\perp}\|^2}{(d_{ij} + Z_{ij,u})^2}} \\
&\approx (d_{ij} + Z_{ij,u})\left(1 + \frac{1}{2}\frac{\|Z_{ij,\perp}\|^2}{(d_{ij} + Z_{ij,u})^2}\right)
\end{aligned} \tag{38}$$

For $\|Z_{ij,u}\| \ll d_{ij}$, we can further approximate:

$$\begin{aligned}
\|q_i - q_j\| &\approx (d_{ij} + Z_{ij,u})\left(1 + \frac{1}{2}\frac{\|Z_{ij,\perp}\|^2}{d_{ij}^2}\right) \\
&\approx d_{ij} + Z_{ij,u} + \frac{\|Z_{ij,\perp}\|^2}{2d_{ij}}
\end{aligned} \tag{39}$$

Since $\|Z_{ij,\perp}\|^2 = \|Z_{ij}\|^2 - Z_{ij,u}^2$, we have:

$$\|q_i - q_j\| \approx d_{ij} + Z_{ij,u} + \frac{\|Z_{ij}\|^2 - Z_{ij,u}^2}{2d_{ij}} \tag{40}$$

Therefore, the deviation can be expressed as:

$$\Delta_{ij} \approx Z_{ij,u} + \frac{\|Z_{ij}\|^2 - Z_{ij,u}^2}{2d_{ij}} \tag{41}$$

The variance of Δ_{ij} can be decomposed as:

$$\begin{aligned}
\text{Var}(\Delta_{ij}) &= \text{Var} \left(Z_{ij,u} + \frac{\|Z_{ij}\|^2 - Z_{ij,u}^2}{2d_{ij}} \right) \\
&= \text{Var}(Z_{ij,u}) + \text{Var} \left(\frac{\|Z_{ij}\|^2 - Z_{ij,u}^2}{2d_{ij}} \right) + 2\text{Cov} \left(Z_{ij,u}, \frac{\|Z_{ij}\|^2 - Z_{ij,u}^2}{2d_{ij}} \right)
\end{aligned} \tag{42}$$

Since $Z_{ij} \sim \mathcal{N}(0, 2\sigma^2 I)$, we have $Z_{ij,u} \sim \mathcal{N}(0, 2\sigma^2)$, thus:

$$\text{Var}(Z_{ij,u}) = 2\sigma^2 \tag{43}$$

For the second term, $\|Z_{ij}\|^2 \sim 2\sigma^2 \chi_3^2$ with variance $12\sigma^4$, and $Z_{ij,u}^2 \sim 2\sigma^2 \chi_1^2$ with variance $8\sigma^4$. The covariance between them is $4\sigma^4$. Therefore:

$$\begin{aligned}
\text{Var} \left(\frac{\|Z_{ij}\|^2 - Z_{ij,u}^2}{2d_{ij}} \right) &= \frac{1}{4d_{ij}^2} \text{Var}(\|Z_{ij}\|^2 - Z_{ij,u}^2) \\
&= \frac{1}{4d_{ij}^2} (\text{Var}(\|Z_{ij}\|^2) + \text{Var}(Z_{ij,u}^2) - 2\text{Cov}(\|Z_{ij}\|^2, Z_{ij,u}^2)) \\
&= \frac{1}{4d_{ij}^2} (12\sigma^4 + 8\sigma^4 - 2 \cdot 4\sigma^4) \\
&= \frac{1}{4d_{ij}^2} (20\sigma^4 - 8\sigma^4) \\
&= \frac{1}{4d_{ij}^2} \cdot 12\sigma^4 \\
&= \frac{3\sigma^4}{d_{ij}^2}
\end{aligned} \tag{44}$$

The third term vanishes due to the independence between $Z_{ij,u}$ and $\|Z_{ij,\perp}\|^2$:

$$\text{Cov} \left(Z_{ij,u}, \frac{\|Z_{ij}\|^2 - Z_{ij,u}^2}{2d_{ij}} \right) = \frac{1}{2d_{ij}} \text{Cov}(Z_{ij,u}, \|Z_{ij,\perp}\|^2) = 0 \tag{45}$$

Hence, the variance of distance deviation is:

$$\text{Var}(\Delta_{ij}) \approx 2\sigma^2 + \frac{3\sigma^4}{d_{ij}^2} \tag{46}$$

For the triplet (p_i, p_j, p_k) , we need to calculate the covariance between deviations Δ_{ij} and Δ_{ik} . The key insight is that $Z_{ij} = R^\top(\eta_i - \eta_j)$ and $Z_{ik} = R^\top(\eta_i - \eta_k)$ share the noise component η_i .

The cross-covariance matrix is:

$$\begin{aligned}
\mathbb{E}[Z_{ij} Z_{ik}^\top] &= \mathbb{E}[R^\top(\eta_i - \eta_j)(\eta_i - \eta_k)^\top R] \\
&= R^\top \mathbb{E}[(\eta_i - \eta_j)(\eta_i - \eta_k)^\top] R
\end{aligned} \tag{47}$$

Expanding the expectation:

$$\begin{aligned}
\mathbb{E}[(\eta_i - \eta_j)(\eta_i - \eta_k)^\top] &= \mathbb{E}[\eta_i \eta_i^\top - \eta_i \eta_k^\top - \eta_j \eta_i^\top + \eta_j \eta_k^\top] \\
&= \mathbb{E}[\eta_i \eta_i^\top] - \mathbb{E}[\eta_i \eta_k^\top] - \mathbb{E}[\eta_j \eta_i^\top] + \mathbb{E}[\eta_j \eta_k^\top]
\end{aligned} \tag{48}$$

Due to independence of noise vectors, only $\mathbb{E}[\eta_i \eta_i^\top] = \sigma^2 I$ is non-zero. Therefore:

$$\begin{aligned}\mathbb{E}[(\eta_i - \eta_j)(\eta_i - \eta_k)^\top] &= \sigma^2 I - 0 - 0 + 0 = \sigma^2 I \\ \mathbb{E}[Z_{ij}Z_{ik}^\top] &= R^\top \sigma^2 I R = \sigma^2 I\end{aligned}\tag{49}$$

This leads to the covariance between projections:

$$\begin{aligned}\text{Cov}(Z_{ij,u}, Z_{ik,u}) &= \mathbb{E}[Z_{ij,u}Z_{ik,u}] - \mathbb{E}[Z_{ij,u}]\mathbb{E}[Z_{ik,u}] \\ &= \mathbb{E}[(Z_{ij} \cdot u_{ij})(Z_{ik} \cdot u_{ik})] \\ &= \mathbb{E}[u_{ij}^\top Z_{ij} Z_{ik}^\top u_{ik}] \\ &= u_{ij}^\top \mathbb{E}[Z_{ij} Z_{ik}^\top] u_{ik} \\ &= u_{ij}^\top \sigma^2 I u_{ik} \\ &= \sigma^2 (u_{ij} \cdot u_{ik})\end{aligned}\tag{50}$$

Considering that the linear terms dominate in the deviation expression, we can approximate:

$$\text{Cov}(\Delta_{ij}, \Delta_{ik}) \approx \text{Cov}(Z_{ij,u}, Z_{ik,u}) = \sigma^2 (u_{ij} \cdot u_{ik})\tag{51}$$

The complete 3×3 covariance matrix for triangle edge deviations is:

$$\Sigma = \begin{bmatrix} \text{Var}(\Delta_{ij}) & \text{Cov}(\Delta_{ij}, \Delta_{ik}) & \text{Cov}(\Delta_{ij}, \Delta_{jk}) \\ \text{Cov}(\Delta_{ik}, \Delta_{ij}) & \text{Var}(\Delta_{ik}) & \text{Cov}(\Delta_{ik}, \Delta_{jk}) \\ \text{Cov}(\Delta_{jk}, \Delta_{ij}) & \text{Cov}(\Delta_{jk}, \Delta_{ik}) & \text{Var}(\Delta_{jk}) \end{bmatrix}\tag{52}$$

Substituting the specific expressions:

$$\Sigma = \begin{bmatrix} 2\sigma^2 + \frac{3\sigma^4}{d_{ij}^2} & \sigma^2 (u_{ij} \cdot u_{ik}) & \sigma^2 (u_{ij} \cdot u_{jk}) \\ \sigma^2 (u_{ik} \cdot u_{ij}) & 2\sigma^2 + \frac{3\sigma^4}{d_{ik}^2} & \sigma^2 (u_{ik} \cdot u_{jk}) \\ \sigma^2 (u_{jk} \cdot u_{ij}) & \sigma^2 (u_{jk} \cdot u_{ik}) & 2\sigma^2 + \frac{3\sigma^4}{d_{jk}^2} \end{bmatrix}\tag{53}$$

The deviation vector of the triangle relation matrix is defined as:

$$\Delta D_{ijk} = D'_{ijk} - D_{ijk} = [\Delta_{ij}, \Delta_{ik}, \Delta_{jk}]\tag{54}$$

This vector follows a multivariate normal distribution:

$$\Delta D_{ijk} \sim \mathcal{N}(\mu, \Sigma)\tag{55}$$

with mean vector:

$$\mu = [\mathbb{E}[\Delta_{ij}], \mathbb{E}[\Delta_{ik}], \mathbb{E}[\Delta_{jk}]] = \left[\frac{3\sigma^2}{d_{ij}}, \frac{3\sigma^2}{d_{ik}}, \frac{3\sigma^2}{d_{jk}} \right]\tag{56}$$

and covariance matrix Σ as defined previously.

The Frobenius norm of the deviation matrix is:

$$\|\Delta D_{ijk}\|_F = \sqrt{\Delta_{ij}^2 + \Delta_{ik}^2 + \Delta_{jk}^2}\tag{57}$$

The squared norm follows a non-central chi-squared distribution with 3 degrees of freedom and non-centrality parameter:

$$\begin{aligned}
\lambda &= \|\mu\|^2 \\
&= \left(\frac{3\sigma^2}{d_{ij}}\right)^2 + \left(\frac{3\sigma^2}{d_{ik}}\right)^2 + \left(\frac{3\sigma^2}{d_{jk}}\right)^2 \\
&= 9\sigma^4 \left(\frac{1}{d_{ij}^2} + \frac{1}{d_{ik}^2} + \frac{1}{d_{jk}^2}\right) \\
&= 9\sigma^4 \sum_{(a,b) \in \{(i,j), (i,k), (j,k)\}} \frac{1}{d_{ab}^2}
\end{aligned} \tag{58}$$

For incorrect point correspondences, at least one point is mismatched or belongs to a different rigid body. In this case, the deviation includes both random noise and systematic geometric error:

$$\Delta D_{ijk} \sim \mathcal{N}(\mu + \delta_{\text{sys}}, \Sigma) \tag{59}$$

where $\delta_{\text{sys}} = [\delta_{ij}, \delta_{ik}, \delta_{jk}]$ represents the systematic error vector that typically satisfies $\|\delta_{\text{sys}}\| \gg \sigma$.

Given a threshold ϵ , we define:

$$p_1 = \mathbb{P}(\|\Delta D_{ijk}\|_F < \epsilon \mid \text{correct correspondence}) \tag{60}$$

$$p_2 = \mathbb{P}(\|\Delta D_{ijk}\|_F < \epsilon \mid \text{incorrect correspondence}) \tag{61}$$

Under conditions of sufficient point cloud density, relatively small noise level σ , and significant systematic error $\|\delta_{\text{sys}}\| \gg \sigma$, we can establish that $p_1 > p_2$.

For correct correspondences, $\|\Delta D_{ijk}\|_F^2$ follows a non-central chi-squared distribution with non-centrality parameter $\lambda_1 = \|\mu\|^2$.

For incorrect correspondences, $\|\Delta D_{ijk}\|_F^2$ follows a non-central chi-squared distribution with non-centrality parameter $\lambda_2 = \|\mu + \delta_{\text{sys}}\|^2$.

Since $\|\delta_{\text{sys}}\| \gg \|\mu\|$, we have $\lambda_2 \gg \lambda_1$. The cumulative distribution function of a non-central chi-squared distribution decreases with increasing non-centrality parameter for a fixed threshold. Therefore:

$$p_1 = \mathbb{P}(\|\Delta D_{ijk}\|_F < \epsilon \mid \text{correct}) \gg \mathbb{P}(\|\Delta D_{ijk}\|_F < \epsilon \mid \text{incorrect}) = p_2 \tag{62}$$

For a k -truss, where each edge is supported by at least $k-2$ triangles, the probability of correctly identifying a correspondence increases exponentially with k , while the probability of incorrectly accepting a false correspondence decreases exponentially. Assuming approximate independence between triangles supporting an edge, the probability of correctly identifying a correspondence with $m = k-2$ supporting triangles is:

$$P(\text{correct} \mid m \text{ triangles}) \approx 1 - (1 - p_1)^m \tag{63}$$

Similarly, the probability of incorrectly accepting a false correspondence with m supporting triangles is:

$$P(\text{incorrect accepted} \mid m \text{ triangles}) \approx (p_2)^m \tag{64}$$

Since $p_1 > p_2$, as m increases (higher k -truss order), the discrimination power between correct and incorrect correspondences increases substantially. This provides the theoretical foundation for why triangle-supported k -truss offer exceptional robustness in point cloud registration, particularly in challenging scenarios with noise, outliers, and partial visibility.

A.3 Computational Complexity Analysis

In this section, we provide a systematic comparison of the computational complexity for four representative dense subgraph algorithms commonly used in graph-based correspondence selection: maximum clique [32], maximal clique [48], k -truss (our method), and k -core[35]. As shown in Table 5, this analysis highlights the superior efficiency of k -truss for large-scale point cloud registration.

maximum clique. The maximum clique problem aims to find the largest fully connected subgraph within a given graph. This is a classic NP-complete problem. The number of possible cliques grows exponentially with the number of vertices, making exact computation intractable for large graphs. The time complexity is exponential with respect to the number of nodes, and thus maximum clique algorithms are unsuitable for practical large-scale applications.

maximal clique. A maximal clique is a clique that cannot be extended by including any adjacent vertex; it is not necessarily the largest clique, but it is maximal with respect to set inclusion. Enumerating all maximal cliques in a graph is also computationally demanding, as the number of such cliques can still be exponential in the worst case. As a result, MAC-based methods are robust in theory but suffer from high computational cost and limited scalability.

k -truss (our method). k -truss decomposition efficiently finds a subgraph in which every edge is contained in at least $k - 2$ triangles. The main computational steps are triangle enumeration and iterative edge removal based on triangle support. The overall time complexity is polynomial, typically $O(m^{1.5})$ where m is the number of edges. This makes k -truss much more efficient and scalable than clique-based methods, while still leveraging higher-order geometric consistency (triangles) for robust correspondence selection.

k -core. k -core decomposition identifies the largest subgraph in which every node has at least degree k . It can be computed with a simple iterative node removal process in linear time, $O(m)$. This method is extremely efficient and suitable for very large graphs. However, k -core only considers node degree and ignores triangle or higher-order structures, which can limit its robustness when facing high outlier rates or complex geometric scenarios.

Table 5: Time complexity comparison of dense subgraph algorithms.

Method	Description	Time Complexity	Structural Strength
maximum clique	Largest fully-connected subgraph	Exponential	Strongest, but intractable
maximal clique (MAC)	Maximal fully-connected subgraph	Exponential	Strong, but costly
k -truss	Each edge in $\geq k - 2$ triangles	Polynomial ($O(m^{1.5})$)	Strong (triangle-based)
k -core	Each node degree $\geq k$	Linear ($O(m)$)	Moderate (degree-based)

Both maximum clique and maximal clique approaches impose strict connectivity constraints but have exponential time complexity, making them impractical for large-scale or real-time applications. k -core is extremely efficient but provides only weak structural guarantees. In contrast, k -truss decomposition achieves a favorable balance: it maintains polynomial computational complexity, making it feasible for large-scale graphs, while its triangle-based structure ensures robust inlier selection. This advantage explains the superior efficiency and effectiveness of k -truss in our framework for large-scale point cloud registration. Moreover, parallel k -truss decomposition algorithms can further improve the speed of k -truss extraction, making it even more suitable for large-scale applications.

A.4 Pseudocode for Our Algorithm

The following pseudocode outlines the complete pipeline of **PointTruss**, our robust 3D point cloud registration framework. The overall method consists of four modular stages: (1) consensus voting-based sampling, (2) compatibility graph construction and k -truss decomposition, (3) cluster-wise transformation estimation, and (4) spatial distribution score-based selection. Each stage is further detailed below with interleaved explanation and modular pseudocode.

Algorithm 1 PointTruss

- 1: **Input:** Source point cloud \mathbf{P} , target point cloud \mathbf{Q} , initial correspondences \mathcal{C} , parameters: noise std σ , inlier threshold τ , sampling ratio β , k -truss parameter k , consensus threshold τ_c , compatibility threshold τ_{comp} , NMS radius r_{nms}
- 2: **Output:** Rigid transformation $(\mathbf{R}^*, \mathbf{t}^*)$
- 3: Apply Algorithm 2 to \mathcal{C} with $\tau_c, r_{\text{nms}}, \beta$ to obtain $\mathcal{I}_{\text{sampled}}$
- 4: Let $\mathcal{C}_{\text{sampled}} = \{\mathcal{C}[i] : i \in \mathcal{I}_{\text{sampled}}\}$
- 5: Construct compatibility graph G among $\mathcal{C}_{\text{sampled}}$; add edge between c_i and c_j if $S_{\text{comp}}(c_i, c_j) > \tau_{\text{comp}}$, using noise parameter σ
- 6: Compute adjacency matrix \mathbf{A} of G
- 7: Apply Algorithm 3 to \mathbf{A} with k to get robust clusters $\{\mathcal{N}_m\}$
- 8: **for** each cluster \mathcal{N}_m **do**
- 9: Compute node centrality in cluster to obtain weights w_i
- 10: Estimate candidate transformation $(\mathbf{R}_m, \mathbf{t}_m)$ using centrality-weighted SVD
- 11: **end for**
- 12: Apply Algorithm 4 to all candidate transformations $\{(\mathbf{R}_m, \mathbf{t}_m)\}$ to obtain optimal $(\mathbf{R}^*, \mathbf{t}^*)$
- 13: **return** $(\mathbf{R}^*, \mathbf{t}^*)$

Step 1: Consensus Voting-based Low-scale Sampling.

Given initial correspondences, we first select a subset of high-quality matches via consensus voting and non-maximum suppression (NMS). This improves the precision of the subsequent graph construction.

Algorithm 2 Consensus Voting-based Low-scale Sampling

- 1: **Input:** Correspondences $\mathcal{C} = \{(\mathbf{p}_i^s, \mathbf{p}_i^t)\}_{i=1}^N$, compatibility scores $S_{\text{comp}}(\cdot, \cdot)$, consistency threshold τ_c , NMS radius r_{nms} , sampling ratio β
- 2: **Output:** Sampled correspondence indices $\mathcal{I}_{\text{sampled}}$
- 3: **for** each correspondence $i = 1$ to N **do**
- 4: Compute consensus score S_i using S_{comp} and threshold τ_c (please see Eq. (3))
- 5: **end for**
- 6: **for** each correspondence $i = 1$ to N **do**
- 7: Apply non-maximum suppression to S_i using NMS radius r_{nms} (please see Eq. (5))
- 8: Compute final score S_i^{final} (please see Eq. (6))
- 9: **end for**
- 10: Set $K = \lfloor \beta \cdot N \rfloor$
- 11: Select indices $\mathcal{I}_{\text{sampled}}$ of the top- K correspondences with the highest S_i^{final}
- 12: **return** $\mathcal{I}_{\text{sampled}}$

Step 2: Compatibility Graph Construction and K-Truss Decomposition.

A compatibility graph is built over the sampled correspondences, where edges represent geometric consistency. We then extract structurally robust clusters using k -truss decomposition.

Step 3: Cluster-wise Transformation Estimation.

For each cluster, we estimate a candidate rigid transformation using centrality-weighted SVD. All candidate transformations are subsequently evaluated in the next step.

Step 4: Spatial Distribution Score (SDS) Based Selection.

We score each candidate using SDS, which measures both the alignment quality and spatial spread of inliers, and select the best one for output.

A.5 Hyper-parameter selection

We set the inlier threshold τ to 0.1 for the 3DMatch and 3DLoMatch datasets. For the KITTI dataset, τ is set to 0.6. The sampling ratio β ranges from 0.1 to 0.5. The k -truss parameter k is chosen between 3 and 10. The consensus threshold τ_c is set to 0.9 by default. The compatibility threshold

Algorithm 3 K-Truss Decomposition for Enhanced Structure Detection

- 1: **Input:** Adjacency matrix \mathbf{A} of the compatibility graph among sampled correspondences, truss parameter k
- 2: **Output:** Robust clusters of correspondences $\{\mathcal{N}_m\}$
- 3: Compute triangle support matrix \mathbf{T} using \mathbf{A}
- 4: Identify valid edges $\mathbf{E}_{\text{valid}}$ where triangle support $\geq (k-2)$
- 5: **for** each vertex i **do**
- 6: Extract neighborhood \mathcal{N}_i connected by valid edges
- 7: **if** $|\mathcal{N}_i| \geq k$ **then**
- 8: Add \mathcal{N}_i to the set of robust clusters $\{\mathcal{N}_m\}$
- 9: **end if**
- 10: **end for**
- 11: **return** $\{\mathcal{N}_m\}$

Algorithm 4 Spatial Distribution Score (SDS) Based Transformation Selection

- 1: **Input:** Source points $\mathbf{P} = \{\mathbf{p}_i^s\}_{i=1}^N$, target points $\mathbf{Q} = \{\mathbf{p}_i^t\}_{i=1}^N$, candidate transformations $\{(\mathbf{R}_m, \mathbf{t}_m)\}_{m=1}^M$, inlier threshold τ
- 2: **Output:** Optimal transformation $(\mathbf{R}^*, \mathbf{t}^*)$
- 3: **for** each candidate $(\mathbf{R}_m, \mathbf{t}_m)$ **do**
- 4: Transform source points using $(\mathbf{R}_m, \mathbf{t}_m)$
- 5: Identify inlier set \mathcal{I}_m using threshold τ
- 6: **if** $|\mathcal{I}_m| < 10$ **then**
- 7: Assign SDS score = 0 for this candidate
- 8: **else**
- 9: Compute inlier ratio ρ_{inlier}
- 10: Compute spatial coverage ratio ρ_{coverage}
- 11: Compute inlier alignment error term ρ_{error}
- 12: Compute SDS score (please see Eq. (14–17))
- 13: **end if**
- 14: **end for**
- 15: Select $(\mathbf{R}^*, \mathbf{t}^*)$ with the highest SDS score
- 16: **return** $(\mathbf{R}^*, \mathbf{t}^*)$

τ_{comp} is adjusted according to the noise standard deviation σ . The NMS radius r_{nms} is typically set to 0.1. All hyperparameters are determined based on empirical validation.

A.6 Ablation study of each component

We conducted systematic ablation studies on the 3DMatch and 3DLoMatch datasets to analyze each component of our algorithm. The MAC (Maximal Clique) method was introduced for comparison, ensuring a comprehensive evaluation of our proposed modules. As shown in Table 6, our method demonstrates the effectiveness of the k-truss for point cloud registration. This structure not only improves overall registration accuracy but also enhances robustness. In addition, the consensus voting-based low-scale sampling strategy and spatial distribution score each contribute positively in experiments. Results indicate that both strategies can serve as effective components for traditional registration methods, improving their performance in challenging scenarios. Overall, our study confirms the practical value and broad applicability of these modules in point cloud registration tasks.

A.7 Limitations and broader impacts

We propose a novel point cloud registration method based on the k-truss in graph theory. This method uses triangles as core constraints and introduces a new perspective for point cloud registration. It fully exploits the advantages of higher-order structures in modeling spatial relationships. Our method performs well in both dense and sparse point cloud scenarios. It shows strong robustness and generalization, effectively resisting high ratios of outliers and noise. In addition, the k-truss decomposition module in our algorithm is highly extensible. It can be used as an independent

Table 6: Analysis experiments on 3DMatch and 3DLoMatch with FPFH and FCGF descriptors. **CV**: Consensus Voting-based Low-scale Sampling Strategy; **MAC**: Maximal Clique; **SDS**: Spatial Distribution Score.

CV	MAC	k-truss	SDS	inlier	RR _{3DMatch} (%)	RR _{3DLoMatch} (%)
FPFH						
1)		✓		✓	83.67	37.10
2)	✓	✓		✓	83.80	38.85
3)		✓		✓	83.73	39.02
4)	✓	✓		✓	84.20	38.91
5)			✓	✓	83.86	37.79
6)	✓		✓	✓	84.20	39.98
7)		✓	✓	✓	83.86	38.85
8)	✓		✓	✓	84.70	43.96
FCGF						
1)		✓		✓	91.68	57.44
2)	✓	✓		✓	93.59	59.46
3)		✓		✓	93.53	59.01
4)	✓	✓		✓	93.72	59.96
5)			✓	✓	93.40	58.00
6)	✓		✓	✓	93.72	59.63
7)		✓	✓	✓	93.66	59.40
8)	✓		✓	✓	93.84	61.64

component and flexibly integrated into other registration algorithms or point cloud processing frameworks, further enhancing overall system performance.

In terms of applications, this method is particularly suitable for scenarios requiring high precision and stability in point cloud registration, such as autonomous driving. For example, in perception and localization tasks for autonomous vehicles, reliable point cloud registration is crucial for environment understanding and high-precision map construction. Nevertheless, our method still has room for improvement in the adaptive selection of the k value and the screening of the optimal k -truss subgraph. At present, how to automatically determine the best k value according to different data characteristics, and how to efficiently select representative k -truss substructures, are the main directions for our future research.

In the future, we will further explore the potential of higher-order topological structures, such as quadrilaterals, in point cloud registration. This will improve the expressive power of the algorithm in complex scenarios. We also plan to leverage high-performance parallel computing frameworks, such as PyTorch, to parallelize the k -truss decomposition process. This will enable real-time processing of large-scale point cloud data. Through these improvements, we aim to promote the application of graph-based point cloud registration algorithms in real engineering scenarios and advance development in related fields.

A.8 Scalability of our algorithm

Our experimental results demonstrate that the proposed algorithm achieves state-of-the-art performance in both accuracy and robustness, while also exhibiting excellent efficiency. With further optimization, such as leveraging PyTorch’s parallel computation capabilities, the speed of our method can be further improved. Currently, the k -truss decomposition accounts for most of the runtime. Several studies have optimized parallel k -truss decomposition, and these techniques can also be applied to our method. In addition, our method can serve as a flexible module that integrates with conventional or deep learning-based descriptors. The proposed Spatial Distribution Score can also be adopted by other methods to further enhance overall accuracy.

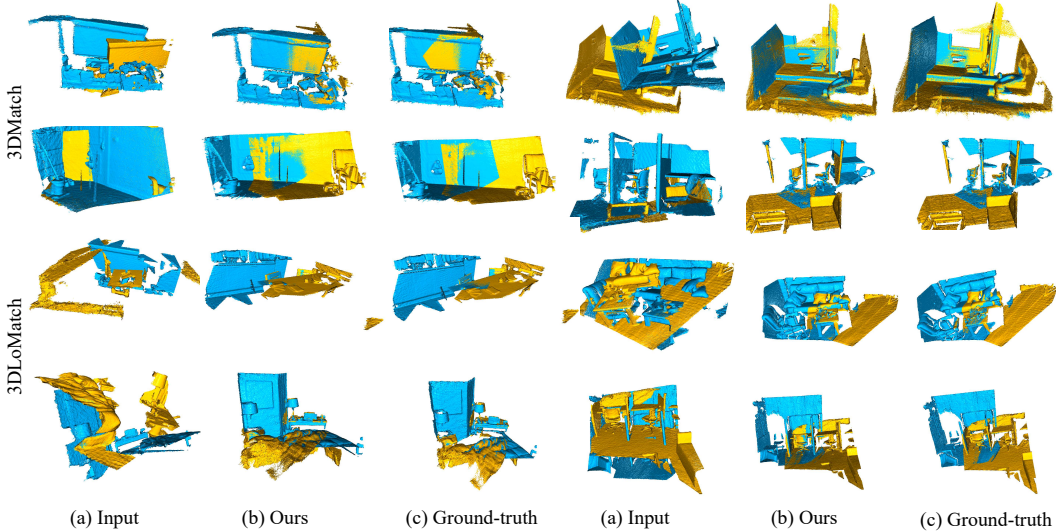


Figure 6: **Visualizations of registration results on the 3DMatch and 3DLoMatch datasets.** The first two rows show examples from 3DMatch, and the last two rows show examples from 3DLoMatch. In each group, yellow and blue point clouds represent the source and target, respectively. From left to right: (a) input point cloud pairs, (b) results of our method, and (c) ground-truth alignment.

A.9 Datasets

All datasets used in this work are publicly available. The Bunny model from the Stanford 3D Scanning Repository was acquired using a Cyberware 3030 MS scanner and is restricted to non-commercial use. The KITTI dataset is published under the NonCommercial-ShareAlike 3.0 License and contains 11 sequences captured by a Velodyne HDL-64 3D LiDAR scanner in outdoor driving scenarios. Following the protocol in [5, 48], we use sequences 8–10 for testing. Additionally, we provide the 3DMatch dataset and its corresponding license information, as shown in Table 7, where 3DLoMatch is a subset of 3DMatch.

Table 7: Source datasets for 3DMatch and their corresponding licenses.

Datasets	License
SUN3D [38]	CC BY-NC-SA 4.0
7-Scenes [33]	Non-commercial use only
RGB-D Scenes v.2 [22]	(License not stated)
Analysis-by-Synthesis [36]	CC BY-NC-SA 4.0
BundleFusion [11]	CC BY-NC-SA 4.0
Halber et al. [16]	CC BY-NC-SA 4.0

A.10 Visualization of Registration Results

We present visual registration results on the 3DMatch and 3DLoMatch datasets in Fig. 6. The yellow and blue point clouds represent the source and target, respectively. The first column shows the input point clouds, and the second column displays the point clouds aligned using the ground-truth transformation. Even on the 3DLoMatch dataset with low overlap, our method clearly extracts the key structure and achieves accurate alignment. We also show registration results on the KITTI dataset in Fig. 7. The input source and target point clouds are in different poses. After applying our estimated transformation, the source point cloud is successfully aligned with the target. The result is almost identical to that of the ground-truth transformation.

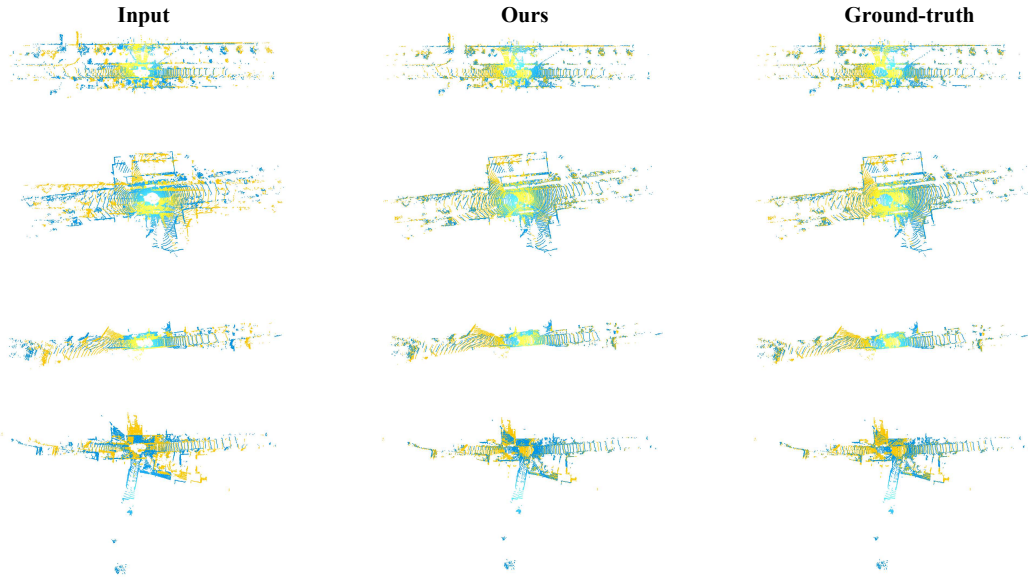


Figure 7: **Visualizations of registration results on the KITTI dataset.** From left to right: input point cloud pairs, registration results using our method, and ground-truth alignment.

A.11 Ablation Study on Graph Sampling and K-value

We conduct comprehensive ablations to evaluate how the sampling ratio β influences accuracy and efficiency, as shown in Table 8.

Table 8: Impact of sampling ratio β on 3DMatch (FCGF).

Sampling Ratio β	Registration Recall	Runtime (s)	Speedup
0.1	93.10%	0.12	8.3 \times
0.2	93.53%	0.16	6.3 \times
0.3	93.84%	0.20	5.0 \times
0.4	93.78%	0.25	4.0 \times
0.5	93.41%	0.31	3.2 \times

Retaining only 10% of correspondences via consensus voting preserves 93.10% registration success while yielding an 8.3 \times speedup, indicating that voting preferentially keeps geometrically consistent correspondences. Higher sampling ratios can be slightly worse than $\beta=0.3$ because they retain more erroneous correspondences that adversely affect the downstream k-truss decomposition.

Initial graph: 5,020 nodes \rightarrow after voting: 502 nodes \rightarrow adjacency: 502 \times 502 with 43,571 edges.

Table 9: K-Truss decomposition statistics with 10% sampling.

k-value	Subgraphs	Node Range	Avg. Nodes
3	502	[3–322]	173.6
4	502	[4–322]	173.6
5	499	[5–322]	174.5
6	498	[6–322]	174.7
7	495	[7–320]	175.5
8	493	[8–321]	176.0
9	492	[9–320]	176.1
10	490	[10–320]	176.4

As shown in Table 9, even with aggressive 10% sampling, subgraphs remain large (average 170+ nodes), due to: (i) high-quality input after the voting pre-filter that enforces strong geometric consistency and high connectivity density; and (ii) natural clustering of correct correspondences, which form richly supported triangle structures satisfying k-truss constraints.

Sensitivity to k and Multi- k The sensitivity of registration recall to k is shown in Table 10.

Table 10: Sensitivity of registration recall to k on 3DMatch with FCGF.

k-value	Registration Recall
3	93.15%
5	93.21%
7	93.59%
10	93.40%
Multi- k (3–10)	93.84%

Performance is weakly sensitive to k because stricter k -truss subgraphs are nested subsets of those at smaller k , forming a natural hierarchy. The multi- k strategy leverages this property. In practice, we select the transformation from the subgraph with the highest spatial distribution score; a global re-estimation using all inliers is unnecessary, as the selected subgraph already yields robust alignment.